Current and projected patterns of warming and marine heatwaves in the Southern Indian Ocean

Clara Azarian, Laurent Bopp, Alice Pietri, Jean-Baptiste Sallée, Francesco d'Ovidio

Current and projected patterns of warming and marine heatwaves in the Southern Indian Ocean

Clara Azarian[1,2], Laurent Bopp[3], Alice Pietri[4], Jean-Baptiste Sallée[1], Francesco d'Ovidio[1]

1 Sorbonne Université, CNRS, IRD, MNHN, Laboratoire d'Océanographie et du Climat: Expérimentations et Approches Numériques (LOCEAN-IPSL), Paris, France.
2 Ecole Nationale des Ponts et Chaussées (ENPC), Champs-sur-Marne, France.
3 Ecole Normale Supérieure / Université PSL, CNRS, Ecole Polytechnique, Sorbonne Université, Paris, PSL University, Laboratoire de Météorologie Dynamique (LMD-IPSL) Paris, France.
4 Instituto del Mar del Peru (IMARPE), Callao, Peru.

Corresponding author: C. Azarian; clara.azarian@locean.ipsl.fr

Abstract

The Southern Indian Ocean (20-120°E, 70-30°S) hosts an exceptional biodiversity that contributed to the inscription of the French and Australian natural reserves on the UNESCO World Heritage List. This region is a "hot spot" for ocean heat uptake and already experiences intense marine heat waves (MHW), as evidenced in 2011/2012 over the Kerguelen Plateau. In the coming decades, this region is also expected to face supplemental anthropogenic warming, depending on future greenhouse gas emissions, with unknown consequences for its marine ecosystems. Here, we present a regional analysis of ocean warming and MHW based on the analyses of historical observations and Coupled Model Intercomparison Project Phase 6 (CMIP6) climate projections. Consistent with observations over the last decades, we find an intensification through the 21st century of surface warming and MHW over a band located between 40°S and 55°S within the Antarctic Circumpolar Current region. CMIP6 models also project much faster climate velocities (i.e. the speed and direction at which isotherms drift in the wake of climate change) in the mesopelagic (200-1000m) than at the surface (0-200m). Lastly, a comparison between the two Shared Socioeconomic Pathways (SSP1-2.6 and SSP2-4.5) analysed in this study shows much larger changes in the second half of the 21st century for the higher emission scenario. These results suggest that the subantarctic islands will probably be mostly affected by warming and MHW under both scenarios, although committing to SSP1-2.6 could substantially alleviate the pressure on ecosystems in the long term. This study also highlights the need to consider a tri-dimensional environment that may evolve at different paces when designing efficient conservation measures.

Keywords

global climate models, ocean warming, ocean extremes, Southern Indian Ocean

1 Introduction

Ocean circulation. The Southern Indian Ocean (20-120°E, 70-30°S) is characterized by dynamic jets and a system of fronts associated with the Antarctic Circumpolar Current (ACC). The ACC is a strong eastward current (Donohue et al., 2016), driven by strong westerly winds (Rintoul and Naveira Garabato, 2013). As the ACC encounters the Kerguelen Plateau, it divides in several branches, with most of the ACC transport passing north of the Plateau (Park et al., 1991,1993, 2009). A strong jet is also observed through the Fawn Trough, a deep passage across the Plateau at 56°S (Park et al., 2008; Roquet et al., 2009; Van Wijk et al., 2010; Vivier et al., 2015; Figure 1). Northwest of the Southern Indian Ocean, the Agulhas Current, a western boundary current, flows southward along the east coast of Africa. At around 40°S, this flow is split with the Agulhas Return Current transporting water eastward (Lutjharms et al., 2006) and the Agulhas leakage transporting water to the South Atlantic (Schmidt et al., 2021). Generally, the frontal system and the circulation in the Southern Indian Ocean is an important biogeographical driver of phytoplankton and zooplankton communities which are at the basis of rich ecosystems (Hunt et al., 2001; Matsuno et al., 2020; Mishra et al., 2020; Venkataramana et al., 2020; Cotte et al., 2022).

Conservation efforts to protect a rich biodiversity. The Southern Indian Ocean region hosts several endemic species, including large populations of megafauna of high patrimonial and economical value like king penguins, yellow-nosed albatrosses, southern elephant seals, krill, toothfish, and many others (Delord et al., 2014). To protect the rich biodiversity of the Southern Indian Ocean, conservation measures have been implemented both in the exclusive economic zones (EEZs) of the subantarctic islands and in the areas under the Commission for the Conservation of Antarctic Marine Living Resources (CCAMLR). Part of EEZs of the following territories, Prince Edward, Crozet, Kerguelen

and Heard and McDonald's islands, are managed through Marine Protected Areas (MPAs). The French national natural reserve (i.e. managed area with zones under strong or integral protection) within Crozet, Kerguelen and Saint-Paul and Amsterdam EEZ was created in 2006 and extended in 2016. The South African MPA around Prince Edward Islands have been officially implemented in 2013 and according to CCAMLR it contributes to a representative system of MPAs, to be used as a scientific reference for future management plans, to foster the recovery of Patagonian toothfish populations and to reduce the bycatch of toothfish fishery on marine seabirds. The Australian MPA around Heard and McDonald Islands was created in 2002 and has been extended in 2014. In total, 5.8% of the Southern Indian Ocean is covered by MPAs and only within EEZs. The new frontier for conservation is now the vast open ocean region that extends beyond EEZs (Della Penna et al. 2017), known as the "High Seas". A workshop held in 2019 organized by the CCAMLR Scientific Committee developed a scientific work program for pelagic spatial planning in the eastern subantarctic region to investigate the relevance of adding new subantarctic spatial conservation tools in the High Seas of the CCAMLR area (Makhado et al., 2019).

Conservation and climate change. One key step in the design of a conservation plan is the evaluation of threats, including climate change (Meredith et al., 2019). The sector directly northward and within the Antarctic Circumpolar Current (ACC), corresponding to the latitudinal band 30°-50°S, in the Southern Indian Ocean is one of the regions of the world that has experienced the largest increase in ocean heat content in recent decades (Llovel & Terray, 2016; Roemmich et al., 2015; Sallée, 2018; Fox-Kemper et al., 2021). This large heat content increase has been explained by an increased heat uptake in the subpolar region transported northward by Ekman transport and subducted within and north of the ACC (Armour et al., 2016; Frölicher et al., 2015; Morrison et al., 2016; Sallée, 2018). In addition to large-scale processes (> 100 km), finer scale processes (1-100 km), which are key for the Southern Indian Ocean circulation (Kostianoy et al., 2004) and can be expected to intensify (Martinez-Moreno et al., 2019; Martinez-Moreno et al., 2021), could also potentially modulate climate change signal locally, maybe inducing important spatial heterogeneity in the temperature trends (e.g. anomalous

vertical heat transport driven by submesoscale fronts altering oceanic heat uptake, Siegelman et al., 2020).

In the Southern Indian Ocean, species distributions are strongly shaped by the large meridional temperature gradient characterizing the region, which covers a transition zone from the subtropic to the Antarctic. Some species are even living close to their thermal tolerance limit (e.g., icefish, Kock & Everson, 2003; Collins et al., 2010) and it has been observed that warming could have a negative impact on the abundance of subantarctic krill, flagellates and Notothenioid fish (Constable et al. 2014) or even potentially on the juvenile recruitment of Patagonian toothfish (Belchier and Collins, 2008). Climate velocity, that is, the speed and direction at which isotherms drift in the wake of climate change (Loarie et al., 2009), can be a useful tool to study biodiversity redistributions due to climate change (Garcia Molinos et al., 2016). Although there is no specific studies on the Southern Ocean using this tool, there are global studies that tend to show that the Southern Ocean may be a generally « slow-moving » basin compared to other regions (Burrows et al., 2014) but also that there may be an important spatial heterogeneity of this indicator (Brito-Morales et al., 2020).

Given the rich biodiversity and the observed and projected warming trends in the Southern Indian Ocean (Fox-Kemper et al., 2021), there is an urgent need to integrate climate change in biodiversity conservation and management. However, if climate change is increasingly presented as one of the threats on biodiversity in conservation plans, such a threat is rarely quantified and no associated actions are indicated. This issue will also likely be raised in line with the momentum fostered by the negotiations of a treaty on the conservation and sustainable use of marine biodiversity in areas beyond national jurisdiction (BBNJ), notably for the development of MPAs in the High Seas (Ban et al., 2014; Maxwell et al., 2020; Crespo et al., 2020). Despite an increasing awareness that climate change might hinder conservation measures efficiency and despite increasing literature on the need to develop new dynamical tools (Tittensor et al., 2019; Crespo et al., 2020), conservation policies seem to remain only focused on managing direct anthropogenic pressures as long as policy-makers have no concrete and operational courses of action to take into account the impacts of climate change (Wilson et al., 2020).

Current lack of relevant knowledge on climate change for policy-makers. Levers for potential action remain today unclear at the regional level and require a better understanding of climate change related hazards at relevant spatial and temporal scales for conservation (Wiens and Bachelet, 2010 ; Carr et al., 2011; Butt et al., 2016; Jones et al., 2016). Today, a gap remains in a systematic description of local observed and future changes over the entire Southern Indian Ocean.

In this study, we aim at addressing this shortcoming, by presenting a regional analysis of past and future ocean warming based on historical observations and climate projections under different scenarios. Here, we use a combination of decadal observations and CMIP6 simulations over the entire Southern Indian Ocean to estimate current trends and analyse projections to help identifying areas that are most likely to undergo significant temperature changes under two future emission scenarios : Shared Socioeconomic Pathways (SSPs) 1-2.6 (high mitigation scenario) and 2-4.5 (modest mitigation scenario; projected to lead to a global warming in 2100 similar to modelled pathways assuming continuation of policies implemented by the end of 2020; IPCC, 2022). We estimate the average temperature trends and extreme events, both listed as “climatic impact-drivers” of marine ecosystems according to the IPCC Assessment Report 6 (Chen et al., 2021; Cooley et al., 2022). We document average temperature trends in terms of warming patterns (°C/decade) as well as climate velocities (km/decade). This analysis is performed for the ocean surface (0-200 m) and for the mesopelagic (200-1000 m) regions. Extreme events are characterized in terms of marine heatwaves (MHW, Hobday et al., 2016; Frölicher et al., 2018). Su and co-authors (2021) characterized MHW but focusing only on the northern part of the Kerguelen Plateau. Our study extends the MHW analysis to the Southern Indian Ocean and uses CMIP6 models to project the evolution of MHW throughout the 21st century.

Figure 1: Ocean circulation in the Southern Indian Ocean. The mean geostrophic velocity between 1993 and 2020 using AVISO product (https://doi.org/10.48670/moi-00148) is shown (grey arrows). Some specific currents are indicated in blue and the Antarctic Circumpolar Current (ACC) fronts, the Northern

Boundary (NB), Subantarctic Front (SAF), Polar Front (PF), Southern ACC front (SACCF) and the Southern Boundary (SB) are shown in brown (constructed from mean dynamic topography, source: Park and Durand, 2019, Park et al., 2019).

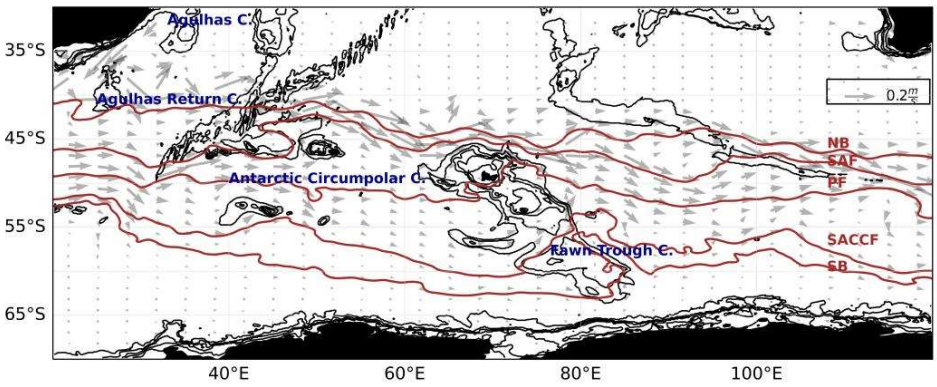

2 Material and Methods

2.1 Data

2.1.1 Observations

The Operational Sea Surface Temperature and Ice Analysis (OSTIA) system run by the UK's Met Office (Good et al., 2020) provides daily sea surface temperature free of diurnal variability at a 0.05deg. x 0.05deg. horizontal grid resolution between 1982 and 2019 (available at

https://marine.copernicus.eu/). This product combines satellite measurements from both infrared and microwave radiometers with in-situ measures from ships, and drifting and moored buoys.

The National Oceanic and Atmospheric Administration Daily Optimum Interpolation Sea Surface Temperature (NOAA OI SST V2 High Resolution) dataset, provided by the NOAA PSL (available from their website at https://psl.noaa.gov), combines sea surface temperature observations (SST at 0.2 m) from different platforms (satellites, ships, buoys and Argo floats) with a 0.25deg x 0.25deg horizontal grid resolution between 1982 and 2019 (Reynolds et al. 2007; Banzon et al. 2016). Contrary to OSTIA dataset, OISST does not include satellite measurements from microwave radiometers as SST inputs (Yang et al., 2021).

2.1.2 *Global climate models – CMIP6*

Models from the Coupled Model Intercomparison Project 6 (CMIP6; Eyring et al., 2016) are used in this study (Table 1). These are coupled ocean-atmosphere models developed by 49 different climate modelling groups[1] that have been used to carry out historical and projection simulations notably to investigate how the Earth system responds to forcing (Eyring et al., 2016).

[1] https://wcrp-cmip.github.io/CMIP6_CVs/docs/CMIP6_institution_id.html

Table 1: CMIP6 models used, using yearly data over multiple depths and daily data at the surface and scenarios associated. CMIP6 models outputs are available at : https://esgf-node.llnl.gov/projects/cmip6/.

	Yearly data – multiple depth levels	**Daily data - surface**	**Ocean horizontal resolution (before interpolation)**	**References**
ACCESS-CM2	Historical,ssp126,ssp245	Historical, ssp126, ssp245	1°	Bi et al., 2020
ACCESS-ESM1-5	Historical, ssp126, ssp245	Historical, ssp126, ssp245	1°	Ziehn et al., 2020
BCC-CSM2-MR	Historical, ssp126,ssp245	Historical, ssp126, ssp245	1°	Wu et al., 2019
CAMS-CSM1-0	Historical, ssp126,ssp245	/	1°	Rong et al., 2019
CanESM5	Historical, ssp126, ssp245	Historical, ssp126, ssp245	1°	Swart et al., 2019; Christian et al., 2021
CanESM5-CanOE	Historical, ssp126, ssp245	/	1°	Swart et al., 2019; Christian et al., 2021
CESM2	Historical, ssp126, ssp245	Historical, ssp126, ssp245	1°	Danabasoglu et al., 2020

CESM2-WACCM	Historical, ssp126, ssp245	Historical, ssp126, ssp245	1°	Danabasoglu et al., 2020
CMCC-CM2-SR5	Historical, ssp126, ssp245	Historical, ssp126, ssp245	1°	Cherchi et al., 2019
CMCC-ESM2	Historical, ssp126, ssp245	Historical, ssp126, ssp245	1°	Lovato et al., 2022
CNRM-CM6-1	Historical, ssp126, ssp245	Historical,ssp126,ssp245	1°	Voldoire et al., 2019
CNRM-CM6-1-HR	/	Historical,ssp126,ssp245	0.25°	Voldoire et al., 2019
CNRM-ESM2-1	Historical, ssp126, ssp245	Historical, ssp126, ssp245	1°	Séférian et al., 2019
GFDL-CM4	Historical, ssp245	Historical, ssp245	0.25°	Held et al., 2019; Dunne et al., 2020
GFDL-ESM4	Historical, ssp126, ssp245	/	0.5°	Dunne et al., 2020
HadGEM3-GC31-LL	Historical, ssp126,ssp245	/	1°	Kuhlbrodt et al., 2018; Andrews et al., 2020
EC-Earth3	/	Historical, ssp126, ssp245	1°	Döscher et al., 2021

EC-Earth3-CC	Historical, ssp245	/	1°	Döscher et al., 2021
EC-Earth3-Veg	Historical, ssp126, ssp245	/	1°	Döscher et al., 2021
IPSL-CM6A-LR	Historical, ssp126, ssp245	Historical, ssp126, ssp245	1°	Boucher et al., 2020
MIROC-6	/	Historical, ssp126, ssp245	1°	Tatebe et al., 2019
MIROC-ES2L	Historical, ssp126, ssp245	/	1°	Hajima et al., 2020
MPI-ESM1-2-HR	Historical, ssp126, ssp245	Historical, ssp126, ssp245	0.4°	Müller et al., 2018; Mauritsen et al., 2019
MPI-ESM1-2-LR	Historical, ssp126, ssp245	Historical, ssp126, ssp245	1.5°	Mauritsen et al., 2019
MRI-ESM2-0	Historical, ssp126, ssp245	Historical, ssp126, ssp245	1°x0.5°	Yukimoto et al., 2019
NESM3	Historical, ssp126, ssp245	Historical, ssp126, ssp245	1°	Cao et al., 2021
UKESM1-0-LL	Historical, ssp126, ssp245	/	1°	Sellar et al., 2019

189

190

Historical and projection simulations from the ScenarioMIP experiments are used. Historical simulations cover the period 1850-2014 and use historical forcing, mostly based on observations, that includes among others greenhouse gas, aerosol concentrations and solar forcing (Eyring et al., 2016). Projection simulations from the ScenarioMIP experiments cover 2015-2100 and over multiple emission trajectories, described through so-called Shared Socioeconomic Pathways (SSPs). More specifically, SSPs describe development pathways according to different economic and political strategies (O'Neill et al., 2017), and subsequent forcing levels similar to the ones used in CMIP5, that are the Representative Concentration Pathways (RCPs). However, SSPs represent an improvement in the sense that those scenarios include updated data on recent emission trends (O'Neill et al., 2016) and allow to explore the implication of different climate change mitigation policies (Riahi et al., 2017). In this study, for all analyses, two projection scenarios are considered: the SSPs 1-2.6 and 2-4.5. The SSP1-2.6 describes a world that shifts to a more sustainable path leading to an estimated warming of 1.8 °C by the end of the century (as compared to pre-industrial) whereas SSP2-4.5 represents a path in which socio-economic trends do not shift significantly from the historical patterns, with an estimated warming of 2.7 °C by the end of the century. The focus on those two scenarios allows the comparison between two possible futures whose occurrence will depend on countries' commitments to reduce their net greenhouse gas emissions (Hausfather & Peters, 2020).

Depending on the analysis, the variable considered is either *thetao* (sea temperature across different depth levels) or *tos* (sea surface temperature) as only *tos* was available daily. Each model output is regridded to the same regular 1°-1° horizontal grid using distance weighted average remapping (using climate data operators « cdo » remapdis) as in Kwiatkowski et al., 2020. Each model output is also regridded vertically following the World Ocean Atlas standard discretization (33 vertical intervals from the surface (0 m) to the abyssal seafloor (5500 m)).

There are several ways to combine the results from multiple models. The traditional approach used by the IPCC, which is the main method used here, is to use a model ensemble mean, all models being weighted equally, and then to study the projections for fixed future periods. For changes in temperature and projected MHW characteristics, future periods of 20 years are considered: the near term (2021-

2040), the mid term (2041-2060) and the long term (2081-2100) as in the IPCC Assessment Report 6 (Chen et al., 2021). An alternative method is also considered to further support the projected trends obtained with the traditional method: the time-shift approach (Herger et al., 2015; Chen et al. 2021; Lee et al., 2021). Instead of specifying a fixed time period, this approach specifies a fixed global warming value compared to pre-industrial, typically 1.5°C, 2°C and 3°C (hereafter referred to as « global warming levels » or GWL 1.5°C, 2°C and 3°C, respectively). These GWLs are in general reached at different time periods depending on the models and on the scenarios. This method allows to account for the different climate sensitivities of the models and facilitates the comparison between global warming and regional spatial patterns. For each model and under each SSP, warming levels are defined as 20-year running means of globally averaged atmospheric surface temperature anomaly compared to the pre-industrial period (1850-1900). Then the change in a given metric (temperature, MHW indicator) is estimated using a climatology of 20 years centred on the first year for which the warming level exceeded a given threshold (e.g., 1.5°C), relative to the 1850-1900 reference value. These results are then averaged over the model ensemble and over the SSPs considered, all simulations being weighted equally. This method is applied to estimate the spatial patterns in warming and in MHW intensity for GWL 1.5°C, GWL 2°C and GWL 3°C. To be able to investigate GWL 3°C, given that not all models for SSP1-2.6 and SSP2-4.5 may reach this threshold, outputs from SSP5-8.5 are also used (Supplementary Figure S1).

Models are also confronted with observations over the historical period for evaluation purposes. More precisely, we evaluate how well the spatial patterns and mean trends are reproduced by the models and compared to observations. This comparison is used as an indicator of what processes affecting trends may be or may not be reproduced by the model ensemble. Such information contributes to the interpretation of projections and uncertainties. Models and observations warming rates and MHW mean intensity are compared respectively over 1982-2019 (to account for natural interannual variability) and 1984-2014 (MHW analysis requiring 30 years of data). CMIP6 historical outputs are thus completed with SSP2-4.5 outputs until 2019, since SSP2-4.5 is most representative of today's emission pathway

(Fricko et al., 2017; Hausfather and Peters, 2020). The temperature trends significance is determined using the coefficient of determination (R^2) of the linear regression as well as a signal-to-noise ratio (SNR) comparing the trend to the interannual variability of the anomaly between the expected (from the linear regression) and observed temperature, as defined in Auger et al., 2021.

To quantify the impact of natural variability on the projected trends, we also exploit additional simulations using the IPSL-CM6A-LR model, which exhibits an important centennial climate variability (Bonnet et al., 2021), through the analysis of the temperature trends of 11 members (r1i1p1f1, r2i1p1f1, r3i1p1f1, r4i1p1f1, r5i1p1f1, r6i1p1f1, r10i1p1f1, r11i1p1f1, r14i1p1f1, r22i1p1f1, r25i1p1f1). These members were all initialized in 1850, but with distinct initial conditions, mostly covering different states regarding the initial trend of the Atlantic Meridional Overturning Circulation (Bonnet et al., 2021). First, the temperature trends over the historical period (1975-2015) of the different members are compared. Second, projected changes in surface temperature for the near, mid and long term periods are compared. Finally, Pearson correlation coefficients between spatial patterns of changes in surface temperature for each member simulation relative to the r1i1p1f1 simulation over each year between 2015 and 2100 in SSP2-4.5 are estimated. The aim is to determine whether the initial conditions of the simulations and natural variability still play an important role in determining the regional characteristics of the projected trends compared to the radiative forcing.

2.2 Climate velocity

For climate velocity we use the classical definition as the ratio between the warming rate and the local spatial gradient of a variable as in Loarie et al., 2009 and Brito-Morales et al., 2018. The intensity of horizontal climate velocity v for temperature (T) is thus here defined as

$$v = \frac{\frac{\partial T}{\partial t}}{||\nabla T||}.$$

By convention, v is positive in case of a warming ($\frac{\partial T}{\partial t}$>0) and negative in case of a cooling.

The climate velocity vector $\vec{v}$ is then defined as

$$\vec{v} = \frac{-\partial T}{\partial t}\left[\frac{\frac{\partial T}{\partial x}}{||\nabla T||^2}.\vec{u}_x + \frac{\frac{\partial T}{\partial y}}{||\nabla T||^2}.\vec{u}_y\right].$$

By convention, $\vec{u}_x$(longitudinal unit vector) is positive eastward and $\vec{u}_y$ (latitudinal unit vector) is positive northward. $\vec{v}$ points to the direction to follow to remain at the same temperature.

For CMIP6 outputs, climate velocity is estimated over different historical periods of 50 years (1850-1900, 1950-2000, 1955-2005 and 1965-2015) to check the sensitivity of the pre-industrial or historical climate velocity that could be used as a baseline for comparison with the projected climate velocities. Then climate velocity is estimated over 2015-2065 and 2050-2100 for SSP1-2.6 and SSP2-4.5, respectively. Climate velocity is estimated for different depth zones: surface (0-200 m) and mesopelagic (200-1000 m). The average temperature weighted by the thickness of each standard depth layer is used to calculate a horizontal climate velocity. The climate velocities obtained from each model are then averaged to get the mean-ensemble results.

2.3 **Marine heatwaves**

The definition of a marine heatwave (MHW) as a "discrete prolonged anomalously warm water event" was introduced in Hobday et al., 2016 to allow for comparison with other studies increasingly adopting this standardized definition. In this work, a MHW is detected when the temperature is above a given threshold for at least 5 days. This threshold is defined as the 90th (for model evaluation) or the 99th percentile (for projections, to focus on the most intense events) of the data distribution. The climatology

and threshold are estimated for each grid point of the region of interest and for each day of the year using an 11-day window. The threshold is also smoothed by applying a 30-day moving average. The climatology is estimated over at least 30 years of data, in order to smooth out climate mode of variability (e.g., ENSO, AMO; Scannell et al., 2016).

MHW can be quantified by different metrics. The definition of MHW intensity varies and can be determined relative to the seasonal climatology or to a chosen threshold (Hobday et al., 2016). Here we define MHW intensity relative to the threshold (90th percentile for model evaluation, 99th percentile for projections) and the mean intensity is weighted by the number of days affected. In addition, the mean number of days affected by MHW per year, also called mean annual MHW days, has been found strongly correlated to some observed ecological performance in the marine environment (e.g., seagrass density, Smale et al., 2019). The two metrics, mean MHW intensity and mean MHW annual days, are therefore used here to characterize MHW as potential climatic impact-drivers of marine ecosystems.

3 Results

3.1. Historical warming trends and marine heatwaves

3.1.1. Warming trends

The mean warming rate observed over the Southern Indian Ocean (20°-120°E, 70°-30°S) between 1982 and 2019 is 0.03°C/decade (±0.08°C/decade, spatial standard deviation), as estimated by a linear regression of observation-based sea surface temperature from the OSTIA product, and 0.07°C/decade (±0.09°C/decade) using OISST dataset (See Section 2.1.1). Such regional averaged temperature trend hides important east/west contrasts (Figure 2, also for OISST as shown in Supplementary Figure S2) with warming trends north of the area and east of the Kerguelen Plateau between 0.1 and 0.3 °C/decade that are found significant (R^2 between 0.4 and 0.5, SNR>1). The cooling pattern west of the Kerguelen

Plateau is not found significant, but has also been obtained on different observational datasets (Yang et al., 2021), suggesting high temporal variability in this area.

In comparison, the 24-single-member-CMIP6-models produces an ensemble mean warming rate from 1982 to 2019 close to the one obtained with OISST dataset (0.085 ± 0.053 °C/decade, spatial standard deviation). A majority of CMIP6 models (17 over 24) simulate higher mean warming rates than the observed one with OISST dataset but none shows an averaged cooling in the region (Figure 2, Supplementary Figure S3). The simulated spatial patterns of temperature trends are quite different between different model simulations, but also between different ensemble members of the same model (IPSL-CM6A-LR, Supplementary Figure S5A). The initial conditions of the simulations as well as decadal and/or multidecadal variability might thus play an important role in the regionalisation of temperature trends over the historical period.

Historical warming rates from the multimodel ensemble are more homogeneous than from any individual models or observations, despite greater warming rates being found between 40° and 50°S north and west of Prince Edward, Marion and Crozet islands (Figure 2). The multimodel ensemble mean underestimates warming trends north of the ACC and east of the Kerguelen Plateau. It shows a general warming throughout the area. A lower signal and/or lower agreement between models is found south of the Kerguelen Plateau near the Antarctic shelves.

Figure 2: Warming rates between 1982 and 2019 in the Southern Indian Ocean, using linear regression on surface temperature, using OSTIA observations (A) and a 24-single-member-CMIP6-model ensemble (B). Hatching indicates areas where the intermodel standard deviation of the warming rate is greater than the mean value, suggesting a low change or a low robustness of the output. For each model and for the 24-model ensemble, the mean warming rate over the area is also calculated and compared to the mean warming rates estimated from the OSTIA and OISST datasets (C). Bars colored in red indicate a higher warming rate than the one derived from OISST (gray bar) and in blue if it is a lower rate.

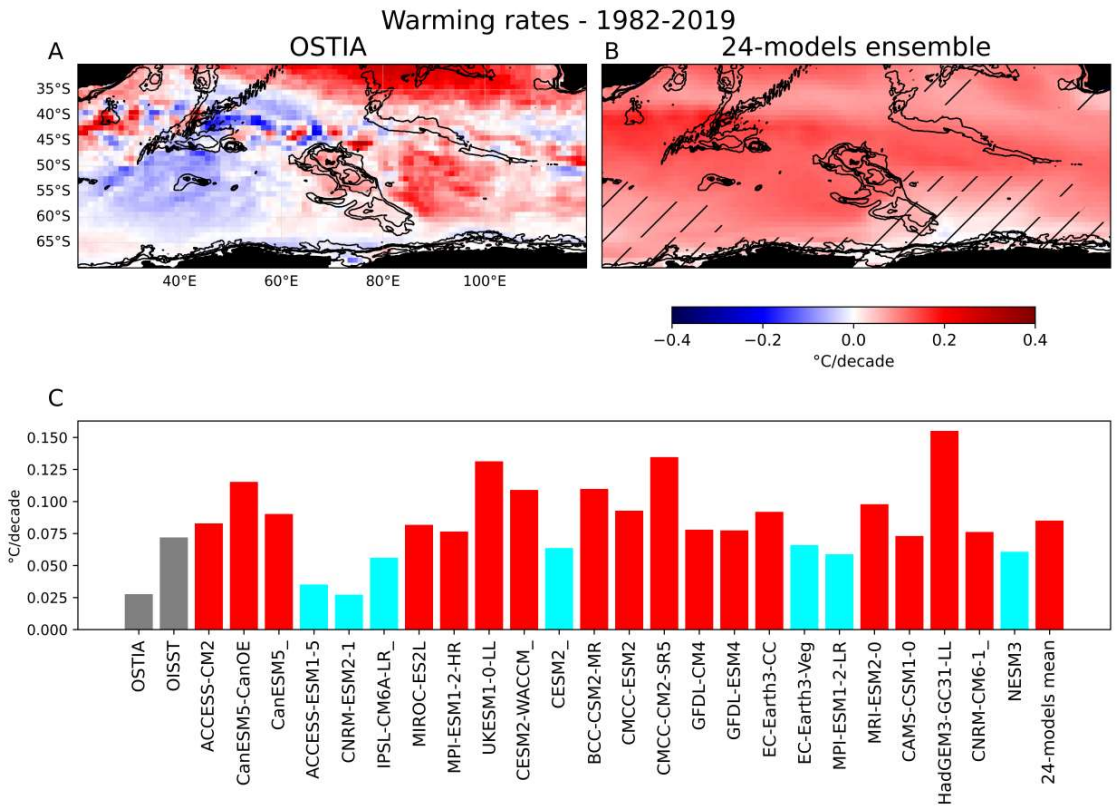

343

344 *3.1.2. Climate velocity*

345

346 The mean climate velocity over the Southern Indian Ocean is 4.9 km/decade (±27 km/decade, spatial
347 standard deviation) using OSTIA dataset and 10.64 km/decade (±34 km/decade) using OISST dataset
348 between 1982 and 2019 (see Sections 2.1.1 and 2.2). An east/west contrast is observed similar to what
349 is found in section 3.1.1. East of the Southern Indian Ocean (70°-120°E, 70°-30°S), the mean climate
350 velocity is around 12 km/decade using OSTIA dataset and around 18 km/decade using OISST dataset.

351

352 *3.1.3. MHW intensity*

353

354 The regional mean MHW intensity observed over the Southern Indian Ocean between 1984 and 2014
355 is 0.35°C above the 90th percentile of the local temperature distribution using the OSTIA dataset
356 (Figure 3). Detection of MHW from the OSTIA dataset highlights a pattern of greater MHW intensity

north of the Kerguelen Plateau, in the region of influence of the ACC (Figure 3, pattern also identified in Su et al., 2021). The 19-model ensemble, reproduced the spatial pattern with greater mean MHW intensity north of the Plateau, notably over the Crozet Plateau, and the less intense MHW west of the Kerguelen Plateau (Figure 3, Supplementary Figure S4).

However, the multimodel mean underestimates the intensity of MHW north of the ACC compared to observations. The mean MHW intensity between 40°S and 30°S obtained from the multimodel mean is 26% lower than the one obtained from observations.

Figure 3: Mean Marine Heatwaves (MHW) intensity as defined by the anomaly above the threshold (90th percentile) between 1984 and 2014 in the Southern Indian Ocean using OSTIA observations (A) and a 19-single-member-CMIP6-model ensemble (B). Hatching indicates areas where the intermodel standard deviation of the MHW intensity is greater than the mean value, suggesting a low robustness of the output.

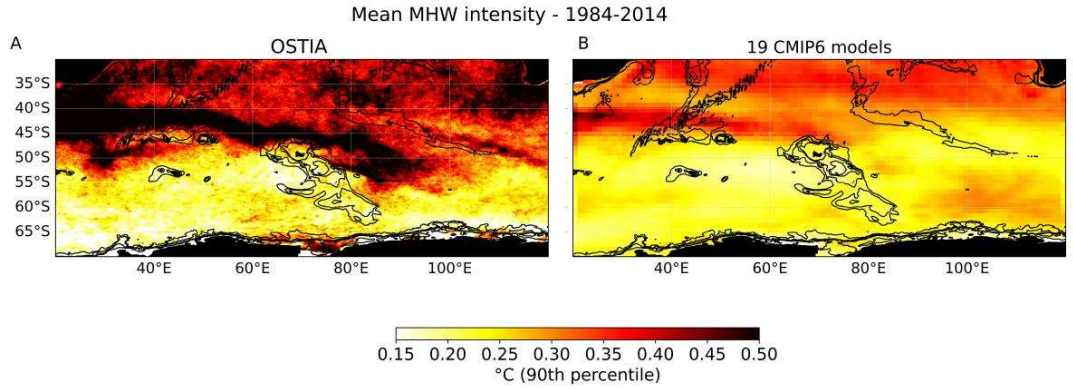

3.2 Projected warming trends and marine heatwaves

3.2.1 The impact of natural variability on the projected temperature trends

To quantify the impact of natural variability on the projected temperature trends, we first focus our analysis on one model (IPSL-CM6A-LR), for which we use an ensemble of simulations and investigate the similarity between members of the simulated patterns for historical and projected warming (see Section 2.1.2).

The mean warming rate over the Southern Indian Ocean varies from 0.031°C/decade to 0.11°C/decade over 1975-2015 between the 11 members of IPSL-CM6A-LR (Supplementary Figure S5). Important differences regarding the spatial patterns are found, with members producing a general warming throughout the region (e.g. r6i1p1f1), others showing a cooling north of the area (e.g. r3i1p1f1, r4i1p1f1, r22i1p1f1) or a cooling east of the Kerguelen Plateau (e.g. r2i1p1f1,r14i1p1f1,r25i1p1f1).

Across the ensemble members, the mean change in surface temperature over the Southern Indian Ocean in SSP2-4.5 ranges from 0.15°C to 0.44°C in the near term (2021-2040), from 0.43 to 0.66°C in the mid term (2041-2060) and from 0.83°C to 1.06°C in the long term (2081-2100), as compared to the historical period (1995-2014, Supplementary Figure 5B). The timeseries of Pearson correlation coefficient relative to r1i1p1f1 member pinpoints the increased similarity between the members' patterns, notably from 2050 onward (correlation coefficient mainly over 0.5, Supplementary Figure 5C). It could be that the remaining differences between the members' projections is to be attributed to a non-deterministic component in ocean response, notably intrinsic ocean variability (Dijkstra, 2016).

This suggests that over the historical period the natural variability is strong and drives a large spread of temperature trends between ensemble members. With increasing radiative forcing, this spread decreases, suggesting that the projected long term spatial patterns are not dependent on natural variability.

3.2.2 Projected warming

Over the Southern Indian Ocean and for SSP2-4.5, the projected warming is 0.29°C (±0.06°C, intermodel variability) in the near term (2021-2040), 0.58°C (±0.09°C) in the mid term (2041-2060)

and 1.05°C (±0.15°C) in the long term (2081-2100), compared to the historical period (1995-2014). While the mean surface temperature change is similar in both scenarios in the near term, it is 1.2 and 1.7 times higher for SSP2-4.5 than for SSP1-2.6, in the mid and long term, respectively (Figure 7).

Using the 24-model ensemble, a larger warming is simulated between 40°S and 50°S and up to 55°S, thus in regions including the Indian Ocean subantarctic Exclusive Economic Zones (EEZs, see Figure 4). This latitudinal band of large warming is located in the ACC and expands southward with time and in SSP2-4.5.

Between 35° and 40°S, warming is lower than in the latitudinal band encompassing the subantarctic island's EEZs (warming of 0.3-0.4°C in SSP2-4.5 mid term). South of 55°S, surface temperature changes remain below 1°C even in the long term in SSP2-4.5. The region south of the ACC has been shown to experience lower warming due to the local circulation and stratification change (Armour et al., 2016; Haumann et al., 2020).

Figure 4: Surface temperature change from the historical period (1995-2014) for the mid-term (A and B) and long term (C and D) projected periods under SSP1-2.6 (A and C) and SSP2-4.5 (B and D) using CMIP6 multimodel mean. Contour lines of similar temperature change are indicated in cyan. Hatched areas indicate where the intermodel standard deviation of the temperature change is higher than the mean value, suggesting a less robust output.

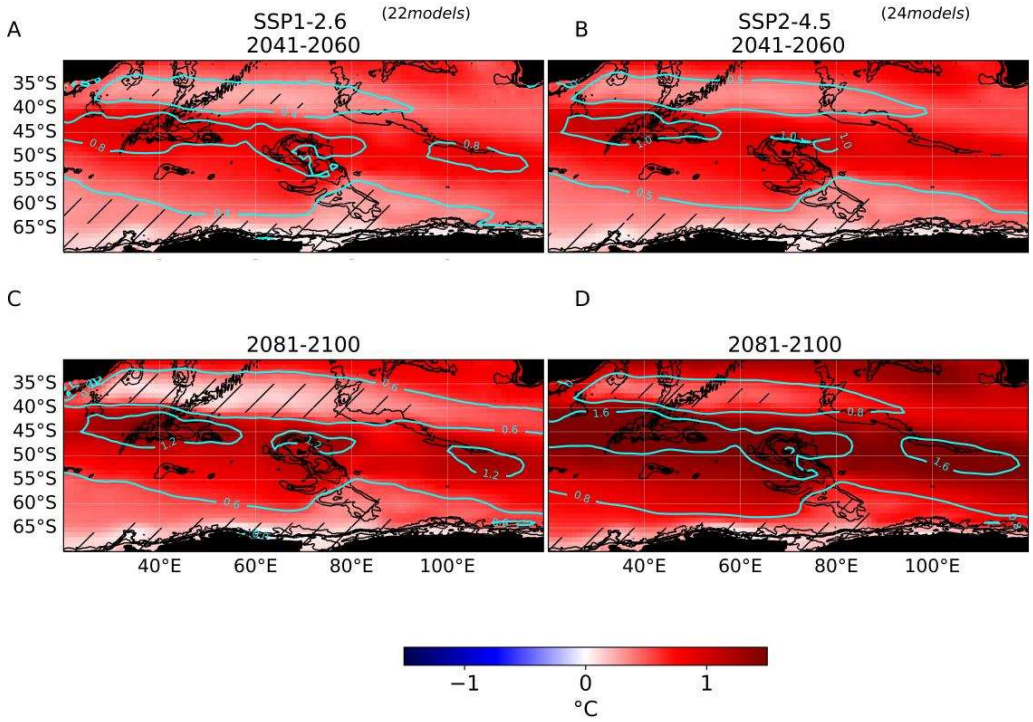

3.2.3 *Projected climate velocity*

For the Southern Indian and in SSP2-4.5, the average climate velocities over 2015-2065 is 38.53 southward (±5.8, intermodel variability) and 47.43 (±8.1) km/decade at the surface and in the mesopelagic, respectively. When averaged over 2050-2100, it is 31.62 (±5.6) and 57.46 (±9.8) km/decade, at the surface and in the mesopelagic, respectively. At the end of the century, surface (mesopelagic) climate velocities are expected to be 5.3 times (1.8 times) faster in SSP2-4.5 as compared to SSP1-2.6 (Figure 7). Mesopelagic climate velocities under both scenarios are also about 5 times faster for the period 2015-2065 compared to the historical period 1955-2005.

Negative surface climate velocities (i.e. northward) over 2050-2100, are found around 35°S in SSP1-2.6 (Figure 5), meaning that this area is expected to cool towards the end of the 21st century. This

cooling is only found at the surface and not at depth under SSP1-2.6, and is not projected under SSP2-4.5.

Important differences are found between surface and mesopelagic climate velocities. Mesopelagic conditions might undergo faster climate velocities than at the surface and that, already over 2015-2050 (Figure 7). For the two projected periods and for both scenarios, mesopelagic climate velocities averaged over the Southern Indian Ocean are between one and four times faster than surface climate velocities. In contrast, for different periods of 50 years between 1850 and 2015, surface climate velocities are found between 1.5 and 3.1 faster than mesopelagic climate velocities. Those differences between climate velocities in the mesopelagic and at the surface are accentuated in some areas. Those differences can reach up to 160 km/decade southwest of Australia, 120 km/decade west of Kerguelen Plateau or vary between 40 and 70 km/decade north of Crozet Plateau in SSP2-4.5. Faster climate velocities in the mesopelagic compared to the surface for a same location (Figure 5) can be due to the weaker spatial temperature gradients at depth as it is for instance the case west of the Australian coast..

Figure 5: Surface (0-200m, A and B) and mesopelagic (200-1000m, C and D) climate velocities, defined as the ratio between the warming rate and the temperature spatial gradient between 2050 and 2100 using multimodel means under SSP1-2.6 (A and C) and SSP2-4.5 (B and D). It can be interpreted as the velocity an individual should adopt to remain at the same temperature. By convention, positive climate velocities correspond to warming trends and negative ones to cooling trends. Black arrows indicate the direction of the climate velocity.

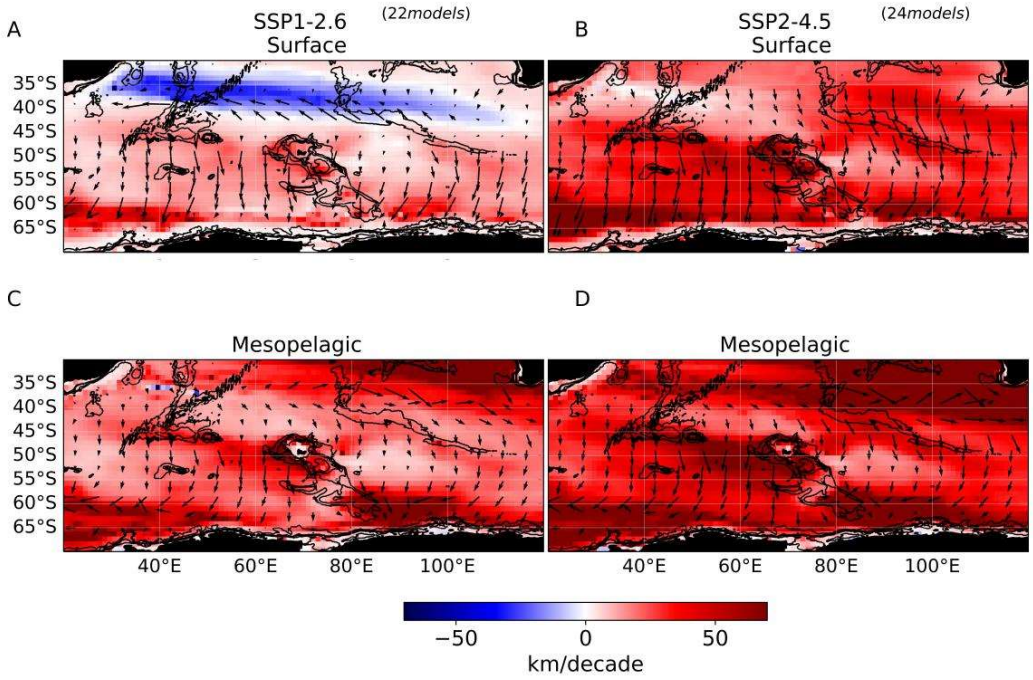

3.2.4 *Projected marine heatwaves*

In the Southern Indian Ocean, the projected mean MHW intensity is 0.28°C (above 99th percentile threshold) in the near term for both scenarios and 0.39°C or 0.63°C in the long term, respectively in SSP1-2.6 or SSP2-4.5. The areas most affected by this intensification in the long term are located between 40°S and 55°S and in particular over Prince Edward, Marion, Crozet, Kerguelen and Heard and McDonald Islands (Figure 6). The spatial pattern of mean MHW intensity in SSP2-4.5 for the near term is similar to the historical pattern (Figure 3). North of the ACC, mean MHW intensity, for this scenario and time horizon, varies between 0.3 and 0.4°C. In the long term under SSP2-4.5, a maximum MHW intensity of 0.97°C is found over Crozet Plateau and the zonal maximum MHW intensity is found to be 0.81°C at 48°S. The pattern obtained is similar to the pattern of surface temperature change (Figure

4), suggesting that the detected MHW might be caused by a mean shift of the temperature distribution rather than a change in the spread of the temperature distribution (as in Oliver et al., 2019a).

Additional analyses, investigating the daily temperature distribution shift in SSP2-4.5 relative to the historical period, show that the relative shift in the mean of the temperature distribution south of 50°S is much larger than the changes in the spread of the distribution, whereas north of 50°S similar orders of magnitude of relative change are found in terms of increased mean temperatures and increased distributions spread (Supplementary Figure S6). In particular, the area between 35° and 40°S shows a larger relative change in the spread of the distribution than in the mean of the distribution, with increases of respectively 9.98% and 7.60% in the long term compared to the historical period.

In the Southern Indian Ocean, the projected mean annual MHW days is 46.1 days/year in the near term and 119.3 days/year in the long term in SSP1-2.6. These values increase to 42.8 days/year and 206 days/year respectively in SSP2-4.5 (Figure 6). Annual MHW days under both scenarios are similar in the near term but it is 23% higher in the mid term and 73% higher in the long term in SSP2-4.5 compared to SSP1-2.6 (Figure 7). Similar as for MHW intensity, the most impacted area is generally the latitudinal zone between 40°S and 55°S in the ACC region. In SSP2-4.5, in the near term, the zonal number of annual MHW days is maximum between 40°S and 55°S varying between 44.5 and 62.9 days, the maximum being reached at 50°S. In the long term, the zonal number of annual MHW days is maximum between 40°S and 57°S varying between 194 and 290 days, the maximum being reached at 51°S. A permanent state of MHW is almost reached over the Kerguelen Plateau (312 days west of the Plateau). When considering the relationship between changes in surface temperatures and MHW annual days for the three projected time periods, it appears that over the whole area a permanent state of MHW could be reached for a 2°C regional mean surface temperature change relative to the historical period (Supplementary Figure S7).

Figure 6: Projected mean MHW intensity (as defined by the anomaly above the threshold of 99th percentile relatively, A and C) and projected mean number of days per year affected by MHW (B and

D) under SSP2-4.5 using a 19-single-member-CMIP6-model ensemble for both 2021-2040 (A and B) and 2081-2100 (C and D). MHW were detected relative to a historical seasonally-varying climatology (1984-2014). Contour lines of similar metric are indicated in cyan. Hatching indicates areas where the intermodel standard deviation of the metric is greater than the mean value, suggesting a low robustness of the output.

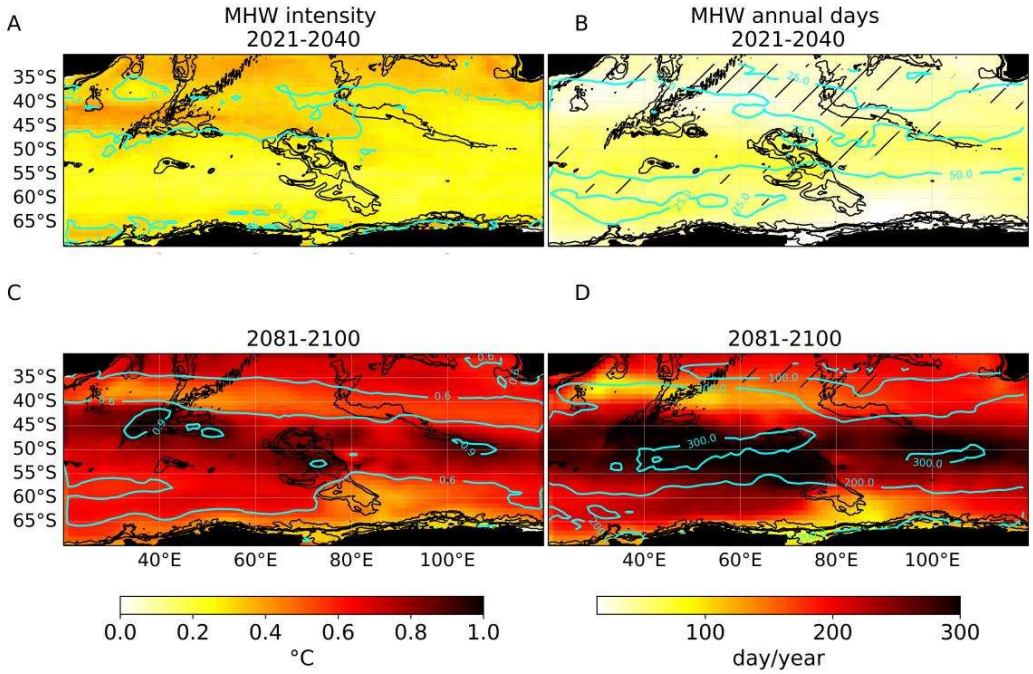

Figure 7: Synthesis of the different climate impact drivers metrics over the Southern Indian Ocean (20°-120°E 70°-30°S) : change in surface temperature (A, relative to 1995-2014); the annual number of day affected by MHW as defined using the 99th percentile threshold (C); average surface (B) and mesopelagic (D) climate velocities. The error bars correspond to the intermodel standard deviation for each metric.

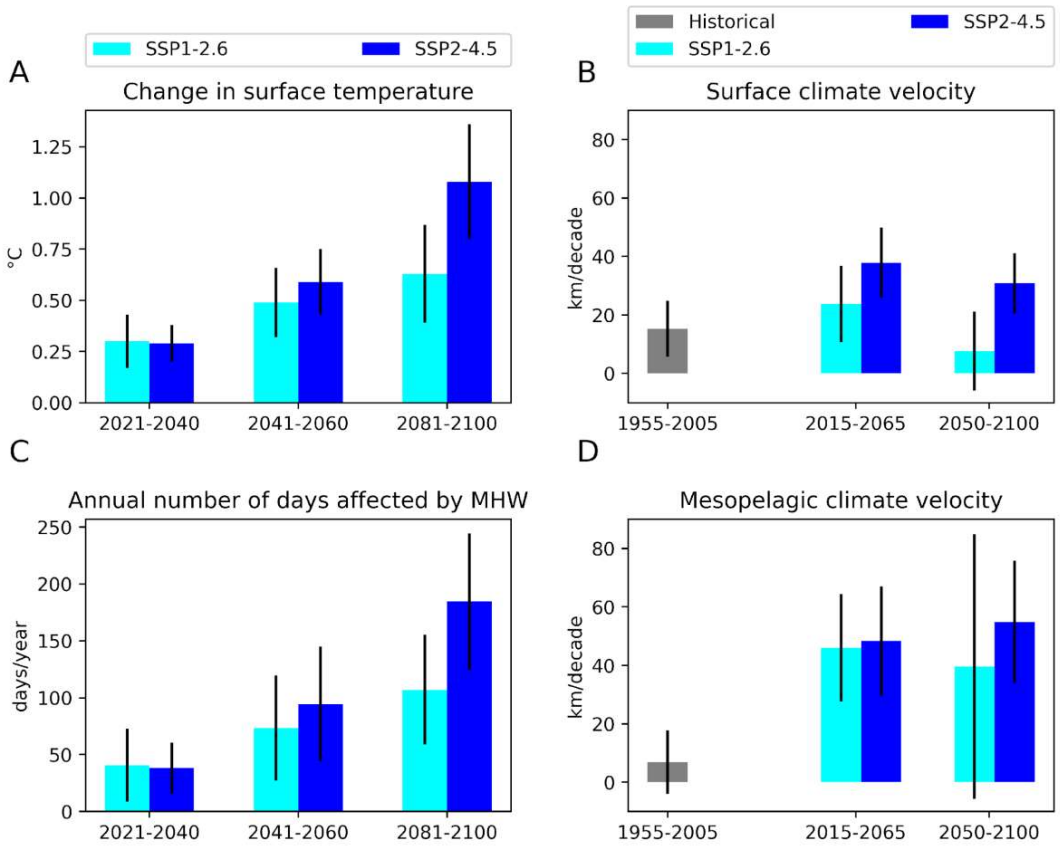

3.3 Patterns of warming-related climatic impact-drivers for GWL 1.5°C, 2°C and 3°C

Patterns of warming-related climatic impact-drivers are also investigated using a timeshift approach (see Section 2.1.2). Not only is this method used to confirm the robustness of the spatial patterns obtained through the traditional approach, but this method also contributes to describing future changes in accordance with targets defined in the Paris Agreement[2], regardless of the mitigation pathway (Chen et al., 2021).

[2] https://unfccc.int/sites/default/files/english_paris_agreement.pdf

The mean sea surface temperature change over the Southern Indian Ocean is 0.6°C (± 0.2°C, intermodel variability), 0.7°C (± 0.2°C) and 1.1°C (± 0.3°C) greater than in 1850-1900 for global warming levels (GWLs, see Section 2.1.2) of 1.5°C, 2°C and 3°C, respectively, as computed from the CMIP6 model ensemble (Figure 8; we remind that GWLs are defined in respect to pre-industrial temperatures and not in respect to the present). In the three cases, the patterns are similar, only the amplitude increases with increasing global warming. Surface temperature changes are warmer than 0.8°C between 40° and 50°S for GWLs 1.5°C and 2°C and warmer than 1.2°C for GWL 3°C at the same latitudes. Surface temperature changes stay below 0.4°C and 0.6°C near the Antarctic, respectively for GWLs 2°C and 3°C.

The mean MHW intensity is 0.37°C (± 0.037°C, intermodel variability), 0.43°C (± 0.050°C) and 0.43°C (± 0.050°C) , for GWLs 1.5°C, 2°C and 3°C, respectively (Figure 8). For GWL 1.5°C, the most intense MHW are found in the subtropical region and north of the ACC (40°-45°S, 20°-90°E) varying between 0.5°C and 0.6°C. For GWLs 2°C and 3°C, mean MHW intensity between 40° and 50°S can be warmer than respectively 0.5°C and 0.8°C. For both warming trends and MHW characteristics, the patterns obtained here using GWLs are similar to the ones obtained using projections on fixed future periods (Section 3.2).

Figure 8: Change in surface temperature for global warming levels (GWLs) 1.5°C (A), 2°C (B) and 3°C (C) and mean MHW intensity for GWLs 1.5°C (D), 2°C (E) and 3°C (F) warming world relative to the pre-industrial period (1850-1900) using a time-shift approach and CMIP6 mean ensembles. The number of simulations used (using SSP1-2.6, SSP2-4.5 and SSP5-8.5) in each case is indicated in parentheses. Contour lines of similar temperature change or MHW intensity are indicated in cyan. Stapling indicates areas where the intermodel standard deviation is higher than the mean value, suggesting a less robust output.

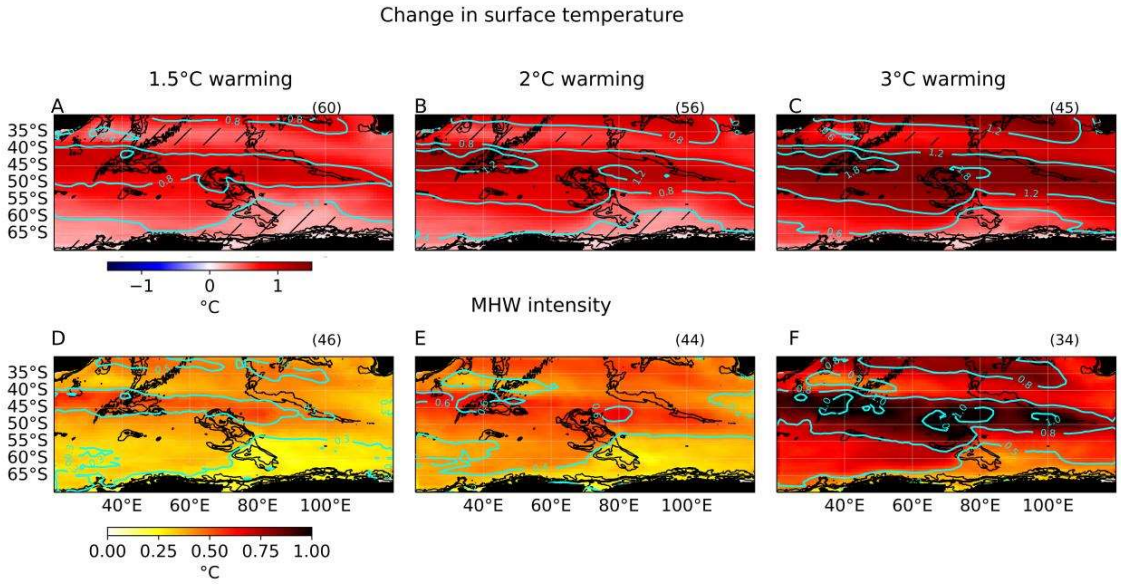

4 Discussion

4.1. Regional characteristics of temperature-related climatic impact-drivers

This study presents a regional analysis of current and projected trends of temperature-related climatic impact-drivers in the Southern Indian Ocean : temperature change, temperature-driven climate velocities and marine heatwaves (MHW). Our main findings can be summarized as follows.

Warming patterns are spatially heterogeneous in the region. Global ocean surface warming rates have been estimated at around 0.08°C/decade between 1880 and 2020 (NOAA, 2022) and the IPCC Assessment Report 6 has indicated a 0.60°C increase in global SST from 1980 to 2020 (Fox-Kemper et al., 2021). In the Southern Indian Ocean, a greater warming north of the Antarctic Circumpolar Current

(ACC) of around 0.11°C/decade has been observed between 1950 and 2012, while cooling patterns have been observed near the Antarctic (Armour et al., 2016; Sallée et al., 2018). The mean warming trend here in the Southern Indian Ocean between 1982 and 2019 is lower, between 0.03°C/decade and 0.07°C/decade (Figure 2, Supplementary Figure S2). Observed warming trends are significant in the northern part of the region and east of Kerguelen Plateau and could vary between 0.1 and 0.3°C/decade.

Climate velocities are faster over Kerguelen Plateau as compared to global ocean averages. The global ocean median climate velocity has been estimated around 13 km/decade over 1900-2010 (Gupta et al., 2015) or 12 km/decade over 1955-2005 (Brito-Morales et al., 2020) at the surface and around 6.3 km/decade in the mesopelagic layer over 1955-2005 (200 - 1000 m). The mean surface climate velocity over the Southern Indian Ocean is found between 4.9 and 10.6 km/decade between 1982 and 2019 using OSTIA and OISST datasets. In particular, surface climate velocities are particularly fast over Heard and McDonalds Islands EEZ (20.3 km/decade, using OSTIA dataset ; 44.0 km/decade, using OISST dataset), Saint-Paul and Amsterdam EEZ (12.9 km/decade ; 24.4 km/decade) and Kerguelen EEZ (11.8 km/decade ; 27.4 km/decade) while they are slower than global estimates or more variable over Crozet EEZ (-2.6 km/decade ; 18.2 km/decade) and Prince Edward Islands EEZ (-5.8 km/decade ; 5.9). Crozet and Prince Edward Islands EEZ are located in the area which seems to undergo a local cooling that could be associated with high temporal variability (Figure 2, Supplementary Figure S2). However, the analyses using IPSL-CM6A-LR members (see Sections 2.1.2 and 3.2.1) suggest that in the long term, radiative forcing will likely dominate warming trends compared to internal variability, and an important warming as well as fast climate velocities are projected over the Crozet Plateau (Section 3.2).

MHW events are particularly intense at the ACC northern boundary between 20°E and 95°E (north of the Kerguelen Plateau). The patterns of MHW mean intensity between 1984 and 2014 obtained with the OSTIA dataset (Figure 3) are consistent with past estimates (Su et al., 2021). However, zooming out from the northern part of the Kerguelen Plateau shows not only that the MHW

are more intense at the northern boundary of the ACC, but also that MHW are generally more intense northward up to the subtropical zone. The global ocean mean intensity of MHW estimated from NOAA observations and defined as the anomaly of temperature compared to the 90th percentile threshold is around 0.35 °C (Plecha & Soares, 2020) when it can reach 1.2°C north of Crozet EEZ.

Over the historical period, no significant spatial contrasts in mean annual MHW days are observed in the Southern Indian Ocean north of 60°S. The global ocean mean annual number of days affected by MHW has been estimated from around 30 days/year in 1900 to around 60 days/year in 2020 (Holbrook et al., 2020, using observations and models). Between 1984 and 2014 using OSTIA dataset, a mean number of around 24 days per year affected by MHW (90th percentile) is observed north of 60°S, with in average 23 annual MHW days over Kerguelen and Crozet EEZ (data not shown). South of 60°S, the mean annual MHW days is lower (16 days/year).

Five contrasted zones emerge. When comparing the projected regional characteristics of both warming and MHW characteristics (climatic impact-drivers), five zones (from the subtropics to the Antarctic continent) associated with specific dynamical features stand out relative to the level of change expected to occur (Figure 9). The first (north of 35°S, subtropical region) and fourth (between 50°S and 55°S, southern part of the ACC) zones are affected by intermediate amplitudes of warming-related climatic impact-drivers. The second (between 35°S and 40°S, under the influence of the Agulhas Return Current) and fifth (south of 55°S, Antarctic colder water) zones have weaker warming and weaker changes in mean MHW intensity and in mean annual MHW days. Finally, the third zone (north of the ACC and covering subantarctic islands) is the one with the most important magnitudes of warming-related climatic impact-drivers, especially over topographic features: the Crozet Plateau, Kerguelen and the Southeastern ridge.

The projected mean MHW intensity might be underestimated in CMIP6. It can be noted that the projected mean MHW intensity might be underestimated, as it was found over the historical period relative to observations (Figure 3) and in global studies using CMIP6 models (Pilo et al., 2019; Plecha et al., 2020). Since the observations suggest that the most intense MHW are related to mesoscale activity and that this mesoscale activity is not always well reproduced by climate models (Pilo et al., 2019; Su et al., 2021), but could be expected to intensify (Hogg et al., 2015; Patara et al., 2016; Martinez-Moreno et al., 2019; Martinez-Moreno et al., 2021), projections in terms of MHW intensity may be underestimated.

Figure 9: Representation of the 5 zones identified in this study in terms of climatic impact-drivers' trends (warming and marine heatwaves) along with the identification of areas for which surface temperature increases by more than 1°C at the end of the century relative to 1995-2014 under SSP1-2.6 and SSP2-4.5; and areas for which mean MHW annual days are higher than 250 day/year at the end of the century under SSP2-4.5 using CMIP6 models. Areas of chlorophyll a concentration greater than 0.25 mg.m-3 (using Copernicus-GlobColour product provided by ACRI-ST company, between 1997 and 2020) are identified in green to allow for comparison between spatialised climate trends and spatialised biological characteristics.

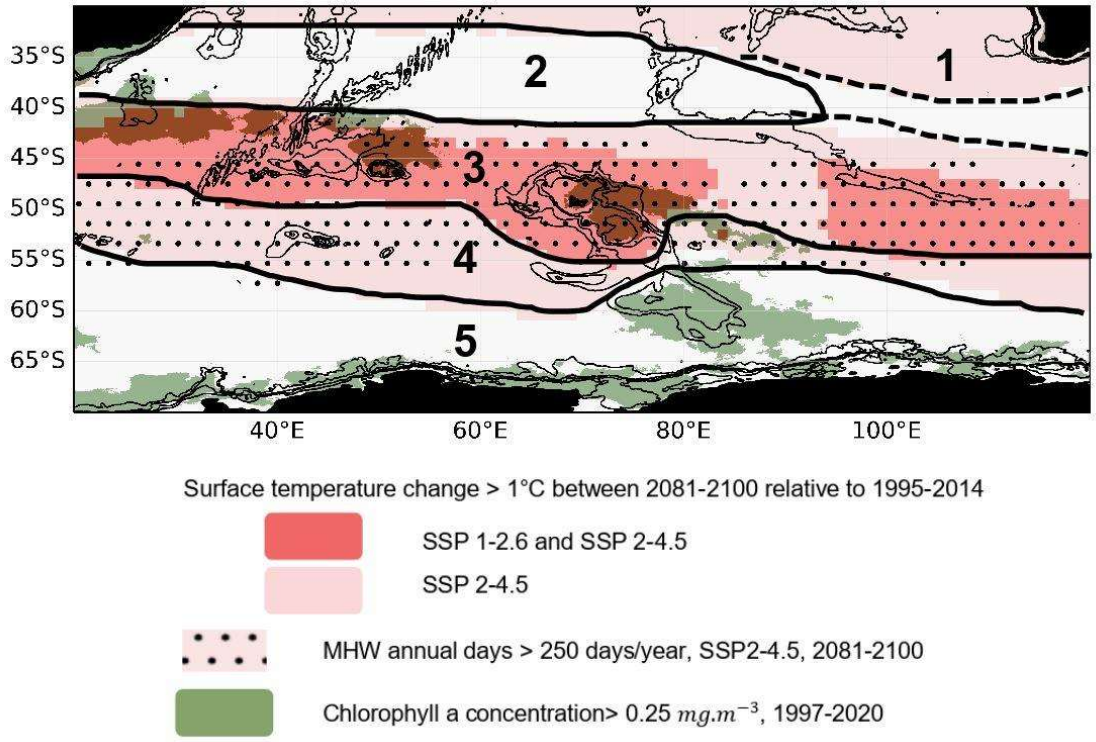

4.2 Implications of climate mitigation

This study also shows how regional patterns of temperature change and marine heatwaves can differ between SSP1-2.6 and SSP2-4.5. Not only can the magnitude of changes be mitigated in SSP1-2.6 but some patterns may be reversed at the end of the century, for instance through the surface cooling obtained around 35°S. However, the major differences between SSP1-2.6 and SSP2-4.5 mainly occurred in the long term.

The consequences of following one SSP instead of another can also be identified at the EEZ scale, both in terms of emerging trends and of magnitude of change. The projected changes in surface temperature over Saint-Paul and Amsterdam EEZ in SSP1-2.6 remain in the range of the observed interannual variability at that location, even in the long term, which is not the case for the other EEZs. Already in the mid term in SSP1-2.6 Crozet, Heard and McDonalds Islands, Kerguelen and Prince Edward Islands

EEZ changes in surface temperature are found to be respectively 2.6, 2.5, 2.8 and 3.1 times higher than the observed (using OSTIA) interannual variability in sea surface temperature (Figure 10). This indicates that emerging warming trends will also occur in a high mitigation scenario (SSP1-2.6) for subantarctic islands.

At the EEZ level, major differences between the two SSPs used in this study mainly occur in the long term. In the long term , the change in surface temperature is 0.62°C , 0.49°C , 0.58°C , 0.65°C and 0.43°C warmer in SSP2-4.5 compared to SSP1-2.6 for Crozet, Heard and McDonalds Islands, Kerguelen, Prince Edward Islands and Saint-Paul and Amsterdam EEZ, respectively. In the long term, mean MHW intensity is 0.39°C , 0.33°C, 0.40°C, 0.40°C and 0.23°C warmer in SSP2-4.5 compared to SSP1-2.6 for respectively Crozet, Heard and McDonalds Islands, Kerguelen, Prince Edward Islands and Saint-Paul and Amsterdam EEZ (Figure 10).

This study therefore shows that the choice of a mitigation strategy and socio-economic development pathway can have direct regional consequences on climate change patterns in the long term, even at the scale of EEZs.

Figure 10: Map of subtropical and subantarctic islands' exclusive economic zones (EEZs) in the Southern Indian Ocean (A). Change in surface temperature relative to 1995-2014 (B), mean MHW intensity (D) and surface (C) and mesopelagic (E) climate velocities averaged over the Southern Indian Ocean (SIO) and different EEZs : Crozet, Heard and Mc Donald Islands (HMI), Kerguelen (KP), Prince Edward Islands (PEI) and Saint-Paul and Amsterdam (SPA), for SSP1-2.6 and SSP2-4.5. Changes in surface temperature and mean MHW intensity are estimated over 2021-2040 (NT), 2041-2060 (MT) and 2081-2100 (LT). Climate velocities were estimated over 2015-2065 (MT) and 2050-2100 (LT). Change in surface temperature results are compared to the observed interannual variability in sea surface temperature in each location calculated from the OSTIA dataset between 1982 and 2019.

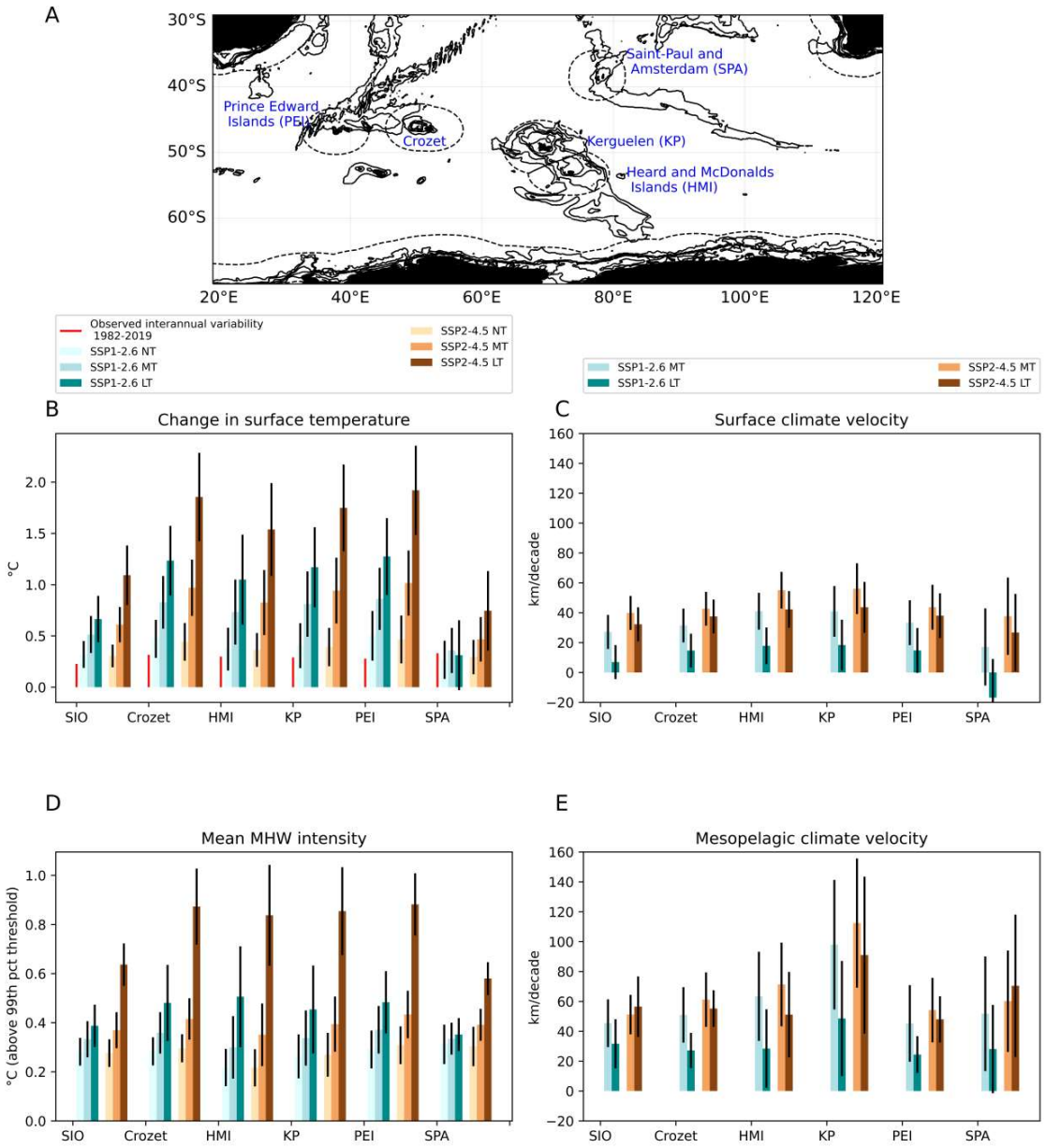

4.3 Coherence with known physical mechanisms and remaining questions

The aim here is to better understand the projected intensities and patterns of warming and marine heatwaves in the Southern Indian Ocean. This requires an evaluation of the models and a mechanistic understanding of the potential heat uptake and redistribution processes.

It can be firstly noted that CMIP6 models have improved compared to CMIP5 models for some key metrics in the Southern Ocean, such as the Antarctic Circumpolar Current (ACC) strength or the representation of differences in density across latitudes of the ACC (Beadling et al., 2020). In addition, the spatial patterns and interannual variability of MHW are better represented in CMIP6 compared to CMIP5 models, and more generally tend to be better represented in higher resolution climate models (Qiu et al., 2021).

There are at least three ways to evaluate a climate model: 1) to compare the model outputs to observation-based products, 2) to verify the agreement between multiple models and/or models' versions (this is done here by using an ensemble of models) and 3) to confront the projections to known physical mechanisms (Baumberger et al., 2017). Given the important role of natural variability for shaping the spatial patterns of historical warming trends, it is difficult to evaluate the quality of the CMIP6 ensemble in simulating warming trends in the Southern Indian Ocean by simply comparing them to past observations (Raäisaänen, 2007; Baumberger et al., 2017; Gopika et al., 2020). We therefore focus here on determining whether the projected patterns of warming and marine heatwaves are coherent with known or potential heat redistribution processes.

The intensity of the Southern Indian Ocean warming is not directly correlated to the intensity of global warming. The models used in our study have a wide range of Equilibrium Climate Sensitivities (ECS; defined as the long term global warming obtained after a doubling of the atmospheric CO_2 above its pre-industrial concentration; Charney et al., 1979; Forster et al., 2021). The ECS of the model ensemble we used in this study vary from 2.29 to 5.62 °C (Forster et al., 2021). However, no correlation was found between the mean ocean warming in the region and the model ECS, that is, models displaying greater warming are not necessarily the ones with greater ECS (data not shown), suggesting that the regional warming in the Southern Indian Ocean is sensitive to local processes, reproduced differently in different models. It is therefore particularly important to investigate whether the projected warming and marine heatwaves patterns in the Southern Indian Ocean can be explained by known physical processes active in the region.

The coherence of the projected patterns of warming-related climatic impact-drivers with known or potential heat redistribution processes is discussed here to both assess the adequacy of the models (Baumberger et al., 2017) and understand their main physical drivers.

4.3.1 The impact of winds and local circulation on warming-related climatic impact-drivers' patterns

CMIP6 projections, either through the traditional or the time-shift approaches (i.e. using GWLs, see Section 2.1.2), suggest an intensification of MHW and warming mostly in the region of influence of the ACC, in the subantarctic latitudinal band between 40° and 55°S. Such result is consistent with the observed increased heat uptake in the subpolar region transported northward by Ekman transport and subducted within and north of the ACC (Armour et al., 2016; Frölicher et al., 2015; Morrison et al., 2016; Sallée, 2018; Huguenin et al., 2022). The strength of this northward Ekman transport is modulated by the position and strength of the westerlies which is particularly strong over the Indian sector of the Southern Ocean (Lin et al., 2018). The westerlies are expected to intensify and to shift poleward (Lee et al., 2021) and thus the associated northward transport of heat content anomaly (anomaly caused by warming) may be strengthened, accumulating heat over the subantarctic (Swart et al., 2018; Fox-Kemper et al., 2021; Silvy et al., 2022). In addition, southward heat transport also occur through eddy advection, partly compensating the Ekman northward heat transport (Farneti et al., 2010; Saenko et al., 2018), but there are still uncertainties on the degree of this compensation (Fox-Kemper et al., 2021).

Another pattern that stands out in this study is the lesser intensification of warming and marine heatwaves between 35° and 40°S. This latitudinal band is mostly under the influence of the Agulhas Current system, which consists in the Agulhas Current, a western boundary current flowing southward along the African coast, which brings warm waters into the Indian Ocean at around 40°S through the Agulhas Return Current up to 70°E (Lutjharms et al., 2006). The remaining waters are transported to

the South Atlantic between 32°S and 42°S and this westerward inflow of relatively warm and salty water exiting the Indian sector is called the Agulhas leakage (Schmidt et al., 2021). Projections from global climate models suggest an increase in Agulhas leakage (Rouault et al., 2009; Backeberg et al., 2012; Biastoch & Böning, 2013), and a decrease of Agulhas Current transport by 11 to 23% at the end of the century (Stellema et al., 2019; Ma et al., 2020; Sen Gupta et al., 2021). If we assume that the decreasing Agulhas Current feeds both the increasing Agulhas leakage and the Agulhas Return Current, and that the Agulhas Current is the main source of water for the Agulhas Return Current, then the Agulhas Return Current would have to decrease. A decreasing Agulhas Return Current would slow down a large heat transport source in the northern part of the Southern Indian Ocean, which could potentially explain the lesser warming projected in this area.

The Agulhas Current system transport is also modulated by the position and strength of the westerlies. Indeed, an equatorward shift of the westerlies (as observed in summer in SSP1-2.6, Bracegirdle et al., 2020) can be associated with an increase of the Agulhas leakage (Durgadoo et al., 2013).

Latitudinal differences in projected warming trends and climate velocities seem therefore consistent with known mechanisms in the region. In particular, the position and strength of the westerlies can have a different effect on a specific zone, depending on how westerlies impact the local circulation.

4.3.2 Remaining questions: on the role of unresolved spatial scales and modes of variability

The projected trends in warming and marine heatwaves therefore seem consistent with potential mechanisms of heat uptake and transport but some key questions remain. Uncertainties remain concerning the role of the ocean mesoscale circulation and the role of the decadal and longer variability.

Finer scale processes (meso- and submesoscale) have the potential to impact warming trends. Eddies can play a significant role in meridional heat transport (Morrison et al., 2016) and can for instance contribute to modulate heat uptake through submesoscale ventilation (Dove et al., 2021). Increased upward heat transport at submesoscale fronts can also alter surface heat uptake capacity (Siegelmann et al., 2020) but the impact of such a process on warming trends locally is yet to be studied. In a changing climate with intensifying winds, it is expected that mesoscale activity might change (Martinez-Moreno et al., 2019; Martinez-Moreno et al., 2021). However, it remains unclear how such changes might also impact the projected warming trends. To investigate whether resolution could play a role in determining the patterns of projected temperature changes, we focus on two models, GFDL-CM4 and MPI-ESM1-2-HR with a resolution of 0.25° and 0.4° respectively. As for the model ensemble, a pattern of greater surface warming over the subantarctic is observed (Supplementary Figure S8). This suggests that the influence of smaller scale processes on the warming patterns may remain limited, at least for the larger eddies represented in higher resolution CMIP6 models. The net impact of eddies on the heat budget and how it will evolve under climate change remain an active field of research (Hewitt et al., 2022).

Internal variability is not negligible in the Southern Indian ocean between 1982 and 2019 but it is challenging to evaluate whether the representation of decadal and multidecadal variability modes and their interaction with the local circulation in the models is accurate. The Southern Indian Ocean is indeed under the influence of various modes of natural variability but depending on the time scale of interest, for instance for policy-makers, different modes of natural variability are to be considered. The Indian Ocean Subtropical Dipole (IOSD) and the El-Niño-Southern Oscillation (ENSO) can influence patterns of SST anomaly (Behera and Yamagata, 2001; Huang and Shuckla, 2008; Morioka et al., 2010) on decadal timescales and the Southern Annular Mode (SAM) on even shorter timescales (Sallée et al., 2010). As the above-mentioned climatic modes of variability may not be in the same phase in reality and in the climate models, this increases the uncertainty on near-term climate projections (Hurrell et al., 2010; Chen et al., 2021).

Multidecadal variability may also not be negligible in the Southern Indian Ocean and could potentially impact projected trends on longer timescales (Zhang et al., 2018). Indeed, the natural variability observed in this study is important over a 37-year period. The east/west contrast obtained in the observations (Section 3.1.1) could result from the response to the positive-to-negative phase transition of the Atlantic Multidecadal Variability (AMV) but the teleconnexion processes associated may not be well represented in climate models (Chung et al., 2022). There are therefore uncertainties on how natural modes of variability and their interactions with the local circulation will evolve, and whether they will enhance, buffer or mask the projected changes.

4.4 Potential impacts on ecosystems

Using the warming-related climatic impact-drivers regional characteristics, it is then important to make the link with the regional ecological characteristics. Here, based on the observed and projected trends in warming and MHW and based on knowledge on the ecology of the Southern Indian Ocean, examples of potential impacts are discussed.

Climate change might induce a shift in habitats for various species, thus potentially affecting the distribution of species with conservation and/or economic values (Reisinger et al., 2022). The region studied here covers three biogeochemical provinces (i.e. oceanographically and ecologically relatively homogeneous regions) as defined by Reygondeau et al., 2020, distributed latitudinally from north to south: the South Subtropical convergence, the Subantarctic water ring and the Antarctic (Reygondeau et al., 2020). Our results suggest that, as far as temperature interactions are concerned, a poleward shift of these provinces is expected and this shift is shown to be faster for the mesopelagic layer compared to the surface with potential ecological impacts for species living across multiple depth layers throughout their life cycle. Such shift between surface and mesopelagic conditions is particularly

relevant for the Saint-Paul and Amsterdam region which is currently located at the transition between different bioregions: the South subtropical convergence in the north and the Subantarctic water ring in the south. By the end of the century, the temperature conditions south of Saint-Paul and Amsterdam EEZ will probably be similar to the ones in the south subtropical convergence province. For the north of the EEZ, the mesopelagic layer temperature conditions will shift faster and could be similar to the ones in the Indian South Subtropical Gyre province. Our study helps identifying other areas that could be undergoing an important shift between surface and mesopelagic conditions and therefore where long term biophysical monitoring could be of special interest: the north-western side of Kerguelen Plateau, slightly up to the southern part of the Crozet Plateau which has been identified as a foraging zone for top predators (e.g. Pütz et al., 2002).

The consequences of the long term shift of thermal conditions in top predators' foraging zones are anticipated by extreme events in the near term (or in the past). The 1997 MHW that occurred in the northern part of the Southern Indian Ocean has been associated with a southward shift of the Polar Front south of the Crozet Plateau where king penguins (*Aptenodytes patagonicus*) from Crozet islands usually forage. The temperature anomaly was so intense and associated with such a major shift of the foraging zones that these zones were barely accessible to the penguins leading to important mortality of those populations (Bost et al., 2015). Over the whole region, the mean MHW intensity of this event remained greater than 0.5°C for 36 days (obtained using OSTIA dataset). Given models projections it appears that such a drastic event may no longer be an extreme phenomenon and if associated with a significant shift in the Polar Front position, it could lead to systematic mass mortality events for top predators.

Intermediate levels of the food webs can also be affected by warming and MHW. Indeed, some populations of fish are already living at the edge of their thermal tolerance. Low-antarctic (i.e. just south of the Antarctic Polar Front) species can live in conditions above their upper optimal range of temperature (1°C to 1.5°C) but further increases in temperature may become too physiologically demanding, especially as the intensification projected appears to occur over their distribution areas (Kock and Everson, 2003).

Besides, a whole range of MHW potential impacts in the Southern Indian Ocean has not yet been covered. Such impacts could include primary production changes (Hayashida et al., 2020), changes in species growth and abundance (Oliver, 2019b; Smale & Wernberg, 2013), changes in population structure (Smale et al., 2017), behavioral changes, notably for reproduction and foraging (Fromant et al., 2021), changes in geographic distributions of species (Cure et al., 2017; Smale & Wernberg, 2013) or even genetic changes (e.g., Coleman et al., 2020). These impacts are yet to be studied in the Southern Indian Ocean.

4.5 Climate change and conservation

A regionalisation of temperature-related climatic impact-drivers, associated with further research on climate change impacts on ecosystems, should contribute to the further consideration of climate change impacts in conservation design and management. Increasing literature aims at addressing this issue and suggests management tools to help integrate climate resilience into MPA design (Tittensor et al., 2019; Crespo et al., 2020). However, efforts are needed to identify the risks posed by climate change at the regional scale. Our study of warming-related climatic impact-drivers mostly addresses the hazards dimension of a risk assessment (which would also include an analysis of the vulnerability and exposure of ecosystems, Chen et al., 2021) and points out the need to include the vertical analysis in the eco regionalisation process, since different layer depths may be impacted differently. In particular, this study shows that the relative difference between mesopelagic and surface climate velocity (a « climatic vertical shear ») is highest over Kerguelen Plateau and Saint-Paul and Amsterdam EEZ under both scenarios while it is the lowest over Heard and McDonalds Islands and Prince Edward Islands EEZ (Figure 10). Yet, mesopelagic climate velocities over Heard and McDonalds Islands and Prince Edward Islands EEZ are still between 20 and 30% faster than surface climate velocities in SSP2-4.5; and respectively between 50% and 60% and between 35% and 66% faster in SSP1-2.6 (Figure 10).

The 3D information provided by climate velocity could be further used to project potential changes in marine biodiversity distribution and help inform conservation management (Arafeh-Dalmau et al., 2021). Through this type of methodology, other concepts related to climate velocity can be used to understand the impact of climate change on species distribution, notably i) climate residence time (Loarie et al., 2009) and ii) climate refugia (Burrows et al., 2014; Brito-Morales et al., 2018). Indeed, it can be useful to know not only if certain environmental conditions will be found and where but also how long these conditions will last in a specific area (climate residence time, Loarie et al., 2009). The concept of climate refugia aims to identify areas that are relatively less impacted by climate change, meaning low climate velocity and/or long climate residence time (Brito-Morales et al., 2018), but it can also be based on the time of emergence of the climate change signal to identify temporary refugia (Bruno et al., 2018). This concept could guide the development of surveillance programs to follow the evolution of environmental conditions on specific zones that are particularly affected by climatic impact-drivers. Climate velocity could also be used to anticipate future expansions of species and to check if current MPA networks cover these expansions (Arafeh-Dalmau et al., 2021). Note that, to be even more biologically meaningful, climate velocity should be combined with other constraints of dispersion such as habitat permeability or connectivity (Brito-Morales et al., 2018). It may also be important to consider multiple variables such as pH (acidification), primary production or zooplankton abundance, since the interaction between multiple variables changes can result in multi-directional distribution shifts (e.g., VanDerWal et al., 2013).

From the characterisation of warming and marine heatwaves patterns presented here, it is difficult to identify potential climate refugia. However, this study pinpoints areas that are scientifically interesting to further study the impacts of climate change on ecosystems, for instance the area south of Crozet near the Antarctic Polar Front and Saint-Paul and Amsterdam EEZ. Indeed, the area south of Crozet, in the main zone of intensification identified in this study, is an important foraging zone for top predators (e.g. Pütz et al., 2002) and is expected to undergo intense warming and increases in MHW intensity and duration but it is also an area that can be subject to important natural variability (as seen on Figure 2). It can therefore be very interesting to study whether this variability in the long term will be enough to

counteract warming trends and whether ecosystems in this area compared to similar ecosystems east of the Kerguelen Plateau (at the same latitudes) will develop different features as a response to different changing conditions. The Saint-Paul and Amsterdam area can also be interesting to protect for further scientific investigation on how the difference between surface and mesopelagic temperature changes might affect endemic ecosystems.

5. Conclusion

The aim of this work is to provide a systematic description of observed and future temperature changes and marine heatwaves over the entire Southern Indian Ocean and to compare the projections over this region under two scenarios that reflect two possible socio-economic pathways.

This analysis shows the spatial heterogeneity of temperature trends and marine heatwaves characteristics at the regional scale, highlighting also some limits. The projected warming trends appear to be consistent with warming mechanisms identified in the literature, notably related to the dynamic of the ACC and the intensification and shifts of westerly winds. Concerning MHW intensity pattern, a better spatial fit between the observations and the models was obtained, although intensities may be underestimated in the models, mainly because of resolution limits, and current spatial patterns of MHW intensity are expected to intensify.

This intensification of both warming and marine heatwaves characteristics is expected to occur mostly over the subantarctic islands, with consequences on endemic species and ecosystems that are still to be further studied. It can be noted that the difference between SSP1-2.6 and SSP2-4.5 projections are mostly significant in the long term, with changes in both scenarios that could be important for ecosystems already in the near and mid term, highlighting the need to anticipate adaptation measures. Such measures would need to also consider that surface and deeper conditions may evolve at different pace.

Through a regional example, this study also reaffirms the need to globally commit to strong mitigation strategies and to follow a sustainable socio-economic development pathway to alleviate the potential impacts of warming and MHW.

Acknowledgements

We acknowledge the World Climate Research Programme's Working Group on Coupled Modelling, that is responsible for CMIP. The authors also thank the IPSL modelling group for the software infrastructure, which facilitated CMIP analysis. We acknowledge funding support from CNES and from the program LEFE led by CNRS-INSU (projects KERTREND and KERTREND-SAT). C.A. was financially supported by the French Ministry of Ecological Transition. A.P. acknowledges the financial support of the Project Concytec - World Bank "Characterization and forecast of extreme events in the Peruvian sea using an operational system of oceanic information", through its executing unit Fondo Nacional de Desarrollo Científico, Tecnológico y de Innovación Tecnológica (Fondecyt). L.B. acknowledges funding from the European Union's Horizon 2020 research and innovation program under grant agreement no. 820989 (project COMFORT).

Declaration of Competing Interest

The authors declare that they have no known competing financial interests or personal relationships that could have appeared to influence the work reported in this paper.

Appendix A : Supplementary material

References

Ab, M. (2019). Expert workshop on pelagic spatial planning for the Eastern Subantartic region (domains 4, 5 and 6). 72.

Andrews, M. B., Ridley, J. K., Wood, R. A., Andrews, T., Blockley, E. W., Booth, B., Burke, E., Dittus, A. J., Florek, P., Gray, L. J., Haddad, S., Hardiman, S. C., Hermanson, L., Hodson, D., Hogan, E., Jones, G. S., Knight, J. R., Kuhlbrodt, T., Misios, S., … Sutton, R. T. (2020). Historical Simulations With HadGEM3-GC3.1 for CMIP6. Journal of Advances in Modeling Earth Systems, 12(6), e2019MS001995. https://doi.org/10.1029/2019MS001995

Arafeh-Dalmau, N., Brito-Morales, I., Schoeman, D. S., Possingham, H. P., Klein, C. J., & Richardson, A. J. (2021). Incorporating climate velocity into the design of climate-smart networks of marine protected areas. Methods in Ecology and Evolution, n/a(n/a). https://doi.org/10.1111/2041-210X.13675

Armour, K. C., Marshall, J., Scott, J. R., Donohoe, A., & Newsom, E. R. (2016). Southern Ocean warming delayed by circumpolar upwelling and equatorward transport. Nature Geoscience, 9(7), 549‐554. https://doi.org/10.1038/ngeo2731

Auger, M., Morrow, R., Kestenare, E., Sallée, J.-B., & Cowley, R. (2021). Southern Ocean in-situ temperature trends over 25 years emerge from interannual variability. Nature Communications, 12(1), 514. https://doi.org/10.1038/s41467-020-20781-1

Ban, N. C., Maxwell, S. M., Dunn, D. C., Hobday, A. J., Bax, N. J., Ardron, J., Gjerde, K. M., Game, E. T., Devillers, R., Kaplan, D. M., Dunstan, P. K., Halpin, P. N., & Pressey, R. L. (2014). Better

integration of sectoral planning and management approaches for the interlinked ecology of the open oceans. Marine Policy, 49, 127‐136. https://doi.org/10.1016/j.marpol.2013.11.024

Banzon, V., Smith, T. M., Chin, T. M., Liu, C., & Hankins, W. (2016). A long‐term record of blended satellite and in situ sea‐surface temperature for climate monitoring, modeling and environmental studies. Earth System Science Data, 8(1), 165‐176. https://doi.org/10.5194/essd‐8‐165‐2016

Baumberger, C., Knutti, R., & Hirsch Hadorn, G. (2017). Building confidence in climate model projections: An analysis of inferences from fit. WIREs Climate Change, 8(3), e454. https://doi.org/10.1002/wcc.454

Beadling, R. L., Russell, J. L., Stouffer, R. J., Mazloff, M., Talley, L. D., Goodman, P. J., Sallée, J. B., Hewitt, H. T., Hyder, P., & Pandde, A. (2020). Representation of Southern Ocean Properties across Coupled Model Intercomparison Project Generations: CMIP3 to CMIP6. Journal of Climate, 33(15), 6555‐6581. https://doi.org/10.1175/JCLI‐D‐19‐0970.1

Behera, S. K., & Yamagata, T. (2001). Subtropical SST dipole events in the southern Indian Ocean. Geophysical Research Letters, 28(2), 327‐330. https://doi.org/10.1029/2000GL011451

Belchier, M., & Collins, M. A. (2008). Recruitment and body size in relation to temperature in juvenile Patagonian toothWsh (Dissostichus eleginoides) at South Georgia. Marine Biology, 155, 493‐503. https://doi.org/10.1007/s00227‐008‐1047‐3

Bi, D., Dix, M., Marsland, S., O'Farrell, S., Sullivan, A., Bodman, R., Law, R., Harman, I., Srbinovsky, J., Rashid, H. A., Dobrohotoff, P., Mackallah, C., Yan, H., Hirst, A., Savita, A., Dias, F. B., Woodhouse, M., Fiedler, R., Heerdegen, A., … Heerdegen, A. (2020). Configuration and spin‐up of ACCESS‐CM2, the new generation Australian Community Climate and Earth System Simulator Coupled Model. Journal of Southern Hemisphere Earth Systems Science, 70(1), 225‐251. https://doi.org/10.1071/ES19040

Bost, C. A., Cotté, C., Terray, P., Barbraud, C., Bon, C., Delord, K., Gimenez, O., Handrich, Y., Naito, Y., Guinet, C., & Weimerskirch, H. (2015). Large-scale climatic anomalies affect marine predator foraging behaviour and demography. Nature Communications, 6(1), 8220. https://doi.org/10.1038/ncomms9220

Boucher, O., Servonnat, J., Albright, A. L., Aumont, O., Balkanski, Y., Bastrikov, V., Bekki, S., Bonnet, R., Bony, S., Bopp, L., Braconnot, P., Brockmann, P., Cadule, P., Caubel, A., Cheruy, F., Codron, F., Cozic, A., Cugnet, D., D'Andrea, F., … Vuichard, N. (2020). Presentation and Evaluation of the IPSL-CM6A-LR Climate Model. Journal of Advances in Modeling Earth Systems, 12(7), e2019MS002010. https://doi.org/10.1029/2019MS002010

Bracegirdle, T.J., Krinner, G., Tonelli, M., Haumann, F. A., Naughten, K. A., Rackow, T., Roach, L. A. and Wainer, I. (2020). Twenty first century changes in Antarctic and Southern Ocean surface climate in CMIP6. Atmos Sci Lett., 21:e984. https://doi.org/10.1002/asl.984

Brito-Morales, I., García Molinos, J., Schoeman, D. S., Burrows, M. T., Poloczanska, E. S., Brown, C. J., Ferrier, S., Harwood, T. D., Klein, C. J., McDonald-Madden, E., Moore, P. J., Pandolfi, J. M., Watson, J. E. M., Wenger, A. S., & Richardson, A. J. (2018). Climate Velocity Can Inform Conservation in a Warming World. Trends in Ecology & Evolution, 33(6), 441‐457. https://doi.org/10.1016/j.tree.2018.03.009

Brito-Morales, I., Schoeman, D. S., Molinos, J. G., Burrows, M. T., Klein, C. J., Arafeh-Dalmau, N., Kaschner, K., Garilao, C., Kesner-Reyes, K., & Richardson, A. J. (2020). Climate velocity reveals increasing exposure of deep-ocean biodiversity to future warming. Nature Climate Change, 10(6), 576‐581. https://doi.org/10.1038/s41558-020-0773-5

Bruno, J. F., Bates, A. E., Cacciapaglia, C., Pike, E. P., Amstrup, S. C., van Hooidonk, R., Henson, S. A., & Aronson, R. B. (2018). Climate change threatens the world's marine protected areas. Nature Climate Change, 8(6), 499‐503. https://doi.org/10.1038/s41558-018-0149-2

Burrows, M. T., Schoeman, D. S., Richardson, A. J., Molinos, J. G., Hoffmann, A., Buckley, L. B., Moore, P. J., Brown, C. J., Bruno, J. F., Duarte, C. M., Halpern, B. S., Hoegh-Guldberg, O., Kappel, C. V., Kiessling, W., O'Connor, M. I., Pandolfi, J. M., Parmesan, C., Sydeman, W. J., Ferrier, S., … Poloczanska, E. S. (2014). Geographical limits to species-range shifts are suggested by climate velocity. Nature, 507(7493), 492- 495. https://doi.org/10.1038/nature12976

Butt, N., Possingham, H. P., De Los Rios, C., Maggini, R., Fuller, R. A., Maxwell, S. L., & Watson, J. E. M. (2016). Challenges in assessing the vulnerability of species to climate change to inform conservation actions. Biological Conservation, 199, 10- 15. https://doi.org/10.1016/j.biocon.2016.04.020

Cai, W., Cowan, T., Godfrey, S., & Wijffels, S. (2010). Simulations of Processes Associated with the Fast Warming Rate of the Southern Midlatitude Ocean. Journal of Climate, 23(1), 197- 206. https://doi.org/10.1175/2009JCLI3081.1

Cao, J., Ma, L., Liu, F., Chai, J., Zhao, H., He, Q., Wang, B., Bao, Y., Li, J., Yang, Y., Deng, H., & Wang, B. (2021). NUIST ESM v3 Data Submission to CMIP6. Advances in Atmospheric Sciences, 38(2), 268- 284. https://doi.org/10.1007/s00376-020-0173-9

Carr, M. H., Woodson, C. B., Cheriton, O. M., Malone, D., McManus, M. A., & Raimondi, P. T. (2011). Knowledge through partnerships : Integrating marine protected area monitoring and ocean observing systems. Frontiers in Ecology and the Environment, 9(6), 342- 350. https://doi.org/10.1890/090096

Cavole, L. M., Demko, A. M., Diner, R. E., Giddings, A., Koester, I., Pagniello, C. M. L. S., Paulsen, M.-L., Ramirez-Valdez, A., Schwenck, S. M., Yen, N. K., Zill, M. E., & Franks, P. J. S. (2016). Biological Impacts of the 2013–2015 Warm-Water Anomaly in the Northeast Pacific. Oceanography, 29(2), 273- 285. JSTOR.

Charney, J. G., Arakawa, A., Baker, D. J., Bolin, B., Dickinson, R. E., Goody, R. M., Leith, C. E., Stommel, H. M., & Wunsch, C. I. (1979). Carbon dioxide and climate: a scientific assessment. Climate Research Board, 13.

Chen, D., M. Rojas, B.H. Samset, K. Cobb, A. Diongue Niang, P. Edwards, S. Emori, S.H. Faria, E. Hawkins, P. Hope, P.Huybrechts, M. Meinshausen, S.K. Mustafa, G.-K. Plattner, and A.-M. Tréguier, 2021: Framing, Context, and Methods. In Climate Change 2021: The Physical Science Basis. Contribution of Working Group I to the Sixth Assessment Report of the Intergovernmental Panel on Climate Change [Masson-Delmotte, V., P. Zhai, A. Pirani, S.L. Connors, C. Péan, S. Berger, N. Caud, Y. Chen, L. Goldfarb, M.I. Gomis, M. Huang, K. Leitzell, E. Lonnoy, J.B.R. Matthews, T.K. Maycock, T. Waterfield, O. Yelekçi, R. Yu, and B. Zhou (eds.)]. Cambridge University Press, Cambridge, United Kingdom and New York, NY, USA, pp. 147–286, doi:10.1017/9781009157896.003.

Cherchi, A., Fogli, P. G., Lovato, T., Peano, D., Iovino, D., Gualdi, S., Masina, S., Scoccimarro, E., Materia, S., Bellucci, A., & Navarra, A. (2019). Global Mean Climate and Main Patterns of Variability in the CMCC-CM2 Coupled Model. Journal of Advances in Modeling Earth Systems, 11(1), 185‐209. https://doi.org/10.1029/2018MS001369

Christian, J. R., Denman, K. L., Hayashida, H., Holdsworth, A. M., Lee, W. G., Riche, O. G. J., Shao, A. E., Steiner, N., & Swart, N. C. (2021). Ocean biogeochemistry in the Canadian Earth System Model version 5.0.3 : CanESM5 and CanESM5-CanOE. Geoscientific Model Development Discussions, 1‐68. https://doi.org/10.5194/gmd-2021-327

Chung, E.-S., Kim, S.-J., Timmermann, A., Ha, K.-J., Lee, S.-K., Stuecker, M. F., Rodgers, K. B., Lee, S.-S., & Huang, L. (2022). Antarctic sea-ice expansion and Southern Ocean cooling linked to tropical variability. Nature Climate Change, 12(5), 461‐468. https://doi.org/10.1038/s41558-022-01339-z

Civel-Mazens, M., Crosta, X., Cortese, G., Michel, E., Mazaud, A., Ther, O., Ikehara, M., & Itaki, T. (2021). Impact of the Agulhas Return Current on the oceanography of the Kerguelen Plateau region, Southern Ocean, over the last 40 kyrs. Quaternary Science Reviews, 251, 106711. https://doi.org/10.1016/j.quascirev.2020.106711

Coleman, M. A., Minne, A. J. P., Vranken, S., & Wernberg, T. (2020). Genetic tropicalisation following a marine heatwave. Scientific Reports, 10(1), 12726. https://doi.org/10.1038/s41598-020-69665-w

Collins, M. A., Brickle, P., Brown, J., & Belchier, M. (2010). Chapter Four - The Patagonian Toothfish : Biology, Ecology and Fishery. In M. Lesser (Éd.), Advances in Marine Biology (Vol. 58, p. 227‑ 300). Academic Press. https://doi.org/10.1016/B978-0-12-381015-1.00004-6

Constable, A. J., Melbourne-Thomas, J., Corney, S. P., Arrigo, K. R., Barbraud, C., Barnes, D. K. A., Bindoff, N. L., Boyd, P. W., Brandt, A., Costa, D. P., Davidson, A. T., Ducklow, H. W., Emmerson, L., Fukuchi, M., Gutt, J., Hindell, M. A., Hofmann, E. E., Hosie, G. W., Iida, T., … Ziegler, P. (2014). Climate change and Southern Ocean ecosystems I : How changes in physical habitats directly affect marine biota. Global Change Biology, 20(10), 3004‑ 3025. https://doi.org/10.1111/gcb.12623

Cooley, S., D. Schoeman, L. Bopp, P. Boyd, S. Donner, D.Y. Ghebrehiwet, S.-I. Ito, W. Kiessling, P. Martinetto, E. Ojea, M.-F. Racault, B. Rost, and M. Skern-Mauritzen (2022). Oceans and Coastal Ecosystems and Their Services. In: Climate Change 2022: Impacts, Adaptation and Vulnerability. Contribution of Working Group II to the Sixth Assessment Report of the Intergovernmental Panel on Climate Change [H.-O. Pörtner, D.C. Roberts, M. Tignor, E.S. Poloczanska, K. Mintenbeck, A. Alegría, M. Craig, S. Langsdorf, S. Löschke, V. Möller, A. Okem, B. Rama (eds.)]. Cambridge University Press, Cambridge, UK and New York, NY, USA, pp. 379–550, doi:10.1017/9781009325844.005.

Cotté, C., Ariza, A., Berne, A., Habasque, J., Lebourges-Dhaussy, A., Roudaut, G., Espinasse, B., Hunt, B.P.V., Pakhomov, E.A., Henschke, N., Péron, C., Conchon, A., Koedooder, C., Izard, L., Cherel, Y. (2022). Macrozooplankton and micronekton diversity and associated carbon vertical patterns and fluxes under distinct productive conditions around the Kerguelen Islands. Journal of Marine Systems, 226, 471-492. https://doi.org/10.1016/B978-0-12-391851-2.00018-0.

Crespo, G. O., Mossop, J., Dunn, D., Gjerde, K., Hazen, E., Reygondeau, G., Warner, R., Tittensor, D., & Halpin. (s. d.). Beyond static spatial management : Scientific and legal considerations for dynamic management in the high seas.

Cure, K., Hobbs, J.-P. A., Langlois, T. J., Abdo, D. A., Bennett, S., & Harvey, E. S. (2017). Distributional responses to marine heat waves : Insights from length frequencies across the geographic

range of the endemic reef fish Choerodon rubescens. Marine Biology, 165(1), 1. https://doi.org/10.1007/s00227-017-3259-x

Danabasoglu, G., Lamarque, J.-F., Bacmeister, J., Bailey, D. A., DuVivier, A. K., Edwards, J., Emmons, L. K., Fasullo, J., Garcia, R., Gettelman, A., Hannay, C., Holland, M. M., Large, W. G., Lauritzen, P. H., Lawrence, D. M., Lenaerts, J. T. M., Lindsay, K., Lipscomb, W. H., Mills, M. J., … Strand, W. G. (2020). The Community Earth System Model Version 2 (CESM2). Journal of Advances in Modeling Earth Systems, 12(2), e2019MS001916. https://doi.org/10.1029/2019MS001916

Della Penna, A., Koubbi, P., Cotté, C., Bon, C., Bost, C.-A., & d'Ovidio, F. (2017). Lagrangian analysis of multi-satellite data in support of open ocean Marine Protected Area design. Future of oceanic animals in a changing ocean, 140, 212‐ 221. https://doi.org/10.1016/j.dsr2.2016.12.014

Delord, K., Barbraud, C., Bost, C.-A., Cherel, Y., Guinet, C., & Weimerskirch, H. (2014). Atlas of top predators from French Southern Territories in the Southern Indian Ocean (p. http://www.cebc.cnrs.fr/ecomm/Fr_ecomm/ecomm_ecor_OI1.html) [Research Report]. CNRS. https://doi.org/10.15474/AtlasTopPredatorsOI_CEBC.CNRS_FrenchSouthernTerritories

Dijkstra, H. (2016). A Normal Mode Perspective of Intrinsic Ocean-Climate Variability. Annual Review of Fluid Mechanics, 48(1), 341‐ 363. https://doi.org/10.1146/annurev-fluid-122414-034506

Donohue, K. A., Tracey, K. L., Watts, D. R., Chidichimo, M. P., and Chereskin, T. K. (2016). Mean Antarctic Circumpolar Current transport measured in Drake Passage. Geophys. Res. Lett., 43, 11760–11767. doi:10.1002/2016GL070319

Döscher, R., Acosta, M., Alessandri, A., Anthoni, P., Arneth, A., Arsouze, T., Bergmann, T., Bernadello, R., Bousetta, S., Caron, L.-P., Carver, G., Castrillo, M., Catalano, F., Cvijanovic, I., Davini, P., Dekker, E., Doblas-Reyes, F. J., Docquier, D., Echevarria, P., … Zhang, Q. (2021). The EC-Earth3 Earth System Model for the Climate ModelIntercomparison Project 6 [Preprint]. Climate and Earth system modeling. https://doi.org/10.5194/gmd-2020-446

Dove, L. A., Thompson, A. F., Balwada, D., & Gray, A. R. (2021). Observational Evidence of Ventilation Hotspots in the Southern Ocean. Journal of Geophysical Research: Oceans, 126(7), e2021JC017178. https://doi.org/10.1029/2021JC017178

Dunne, J. P., Horowitz, L. W., Adcroft, A. J., Ginoux, P., Held, I. M., John, J. G., Krasting, J. P., Malyshev, S., Naik, V., Paulot, F., Shevliakova, E., Stock, C. A., Zadeh, N., Balaji, V., Blanton, C., Dunne, K. A., Dupuis, C., Durachta, J., Dussin, R., … Zhao, M. (2020). The GFDL Earth System Model Version 4.1 (GFDL-ESM 4.1) : Overall Coupled Model Description and Simulation Characteristics. Journal of Advances in Modeling Earth Systems, 12(11), e2019MS002015. https://doi.org/10.1029/2019MS002015

Durgadoo, J. V., Loveday, B. R., Reason, C. J. C., Penven, P., & Biastoch, A. (2013). Agulhas Leakage Predominantly Responds to the Southern Hemisphere Westerlies. Journal of Physical Oceanography, 43(10), 2113‐2131. https://doi.org/10.1175/JPO-D-13-047.1

Eyring, V., Bony, S., Meehl, G. A., Senior, C. A., Stevens, B., Stouffer, R. J., & Taylor, K. E. (2016). Overview of the Coupled Model Intercomparison Project Phase 6 (CMIP6) experimental design and organization. Geoscientific Model Development, 9(5), 1937‐1958. https://doi.org/10.5194/gmd-9-1937-2016

Farneti, R., Delworth, T. L., Rosati, A. J., Griffies, S. M., & Zeng, F. (2010). The Role of Mesoscale Eddies in the Rectification of the Southern Ocean Response to Climate Change. Journal of Physical Oceanography, 40(7), 1539‐1557. https://doi.org/10.1175/2010JPO4353.1

Forster, P., T. Storelvmo, K. Armour, W. Collins, J.-L. Dufresne, D. Frame, D.J. Lunt, T. Mauritsen, M.D. Palmer, M. Watanabe, M. Wild, and H. Zhang (2021). The Earth's Energy Budget, Climate Feedbacks, and Climate Sensitivity. In Climate Change 2021: The Physical Science Basis. Contribution of Working Group I to the Sixth Assessment Report of the Intergovernmental Panel on Climate Change [Masson-Delmotte, V., P. Zhai, A. Pirani, S.L. Connors, C. Péan, S. Berger, N. Caud, Y. Chen, L. Goldfarb, M.I. Gomis, M. Huang, K. Leitzell, E. Lonnoy, J.B.R. Matthews, T.K. Maycock, T.

Waterfield, O. Yelekçi, R. Yu, and B. Zhou (eds.)]. Cambridge University Press, Cambridge, United Kingdom and New York, NY, USA, pp. 923–1054, doi:10.1017/9781009157896.009

Fox-Kemper, B., H.T. Hewitt, C. Xiao, G. Aðalgeirsdóttir, S.S. Drijfhout, T.L. Edwards, N.R. Golledge, M. Hemer, R.E. Kopp, G. Krinner, A. Mix, D. Notz, S. Nowicki, I.S. Nurhati, L. Ruiz, J.-B. Sallée, A.B.A. Slangen, and Y. Yu (2021). Ocean, Cryosphere and Sea Level Change. In Climate Change, 2021. The Physical Science Basis. Contribution of Working Group I to the Sixth Assessment Report of the Intergovernmental Panel on Climate Change [Masson-Delmotte, V., P. Zhai, A. Pirani, S.L. Connors, C. Péan, S. Berger, N. Caud, Y. Chen, L. Goldfarb, M.I. Gomis, M. Huang, K. Leitzell, E. Lonnoy, J.B.R. Matthews, T.K. Maycock, T. Waterfield, O. Yelekçi, R. Yu, and B. Zhou (eds.)]. Cambridge University Press, Cambridge, United Kingdom and New York, NY, USA, pp. 1211–1362, doi:10.1017/9781009157896.011

Frölicher, T. L., Sarmiento, J. L., Paynter, D. J., Dunne, J. P., Krasting, J. P., & Winton, M. (2015). Dominance of the Southern Ocean in Anthropogenic Carbon and Heat Uptake in CMIP5 Models. Journal of Climate, 28(2), 862‐886. https://doi.org/10.1175/JCLI-D-14-00117.1

Frölicher, T. L., Fischer, E. M., & Gruber, N. (2018). Marine heatwaves under global warming. Nature, 560(7718), 360‐364. https://doi.org/10.1038/s41586-018-0383-9

Fromant, A., Delord, K., Bost, C.-A., Eizenberg, Y. H., Botha, J. A., Cherel, Y., Bustamante, P., Gardner, B. R., Brault-Favrou, M., Lec'hvien, A., & Arnould, J. P. Y. (2021). Impact of extreme environmental conditions : Foraging behaviour and trophic ecology responses of a diving seabird, the common diving petrel. Progress in Oceanography, 198, 102676. https://doi.org/10.1016/j.pocean.2021.102676

García Molinos, J., Halpern, B., Schoeman, D. et al. (2016). Climate velocity and the future global redistribution of marine biodiversity. Nature Clim Change 6, 83–88. https://doi.org/10.1038/nclimate2769

Good, S., Fiedler, E., Mao, C., Martin, M. J., Maycock, A., Reid, R., Roberts-Jones, J., Searle, T., Waters, J., While, J., & Worsfold, M. (2020). The Current Configuration of the OSTIA System for Operational Production of Foundation Sea Surface Temperature and Ice Concentration Analyses. Remote Sensing, 12(4), 720. https://doi.org/10.3390/rs12040720

Gopika, S., Izumo, T., Vialard, J., Lengaigne, M., Suresh, I., & Kumar, M. R. R. (2020). Aliasing of the Indian Ocean externally-forced warming spatial pattern by internal climate variability. Climate Dynamics, 54(1- 2), 1093- 1111. https://doi.org/10.1007/s00382-019-05049-9

Hajima, T., Watanabe, M., Yamamoto, A., Tatebe, H., Noguchi, M. A., Abe, M., Ohgaito, R., Ito, A., Yamazaki, D., Okajima, H., Ito, A., Takata, K., Ogochi, K., Watanabe, S., & Kawamiya, M. (2020). Development of the MIROC-ES2L Earth system model and the evaluation of biogeochemical processes and feedbacks. Geoscientific Model Development, 13(5), 2197- 2244. https://doi.org/10.5194/gmd-13-2197-2020

Haumann, F. A., Gruber, N., & Münnich, M. (2020). Sea-Ice Induced Southern Ocean Subsurface Warming and Surface Cooling in a Warming Climate. AGU Advances, 1(2), e2019AV000132. https://doi.org/10.1029/2019AV000132

Hausfather, Z., & Peters, G. P. (2020). Emissions – the 'business as usual' story is misleading. Nature, 577(7792), 618- 620. https://doi.org/10.1038/d41586-020-00177-3

Hayashida, H., Matear, R. J., Strutton, P. G., & Zhang, X. (2020). Insights into projected changes in marine heatwaves from a high-resolution ocean circulation model. Nature Communications, 11(1), 4352. https://doi.org/10.1038/s41467-020-18241-x

Held, I. M., Guo, H., Adcroft, A., Dunne, J. P., Horowitz, L. W., Krasting, J., Shevliakova, E., Winton, M., Zhao, M., Bushuk, M., Wittenberg, A. T., Wyman, B., Xiang, B., Zhang, R., Anderson, W., Balaji, V., Donner, L., Dunne, K., Durachta, J., … Zadeh, N. (2019). Structure and Performance of GFDL's CM4.0 Climate Model. Journal of Advances in Modeling Earth Systems, 11(11), 3691- 3727. https://doi.org/10.1029/2019MS001829

Herger, N., Sanderson, B. M., and Knutti, R. (2015), Improved pattern scaling approaches for the use in climate impact studies. Geophys. Res. Lett., 42, 3486– 3494. doi: 10.1002/2015GL063569.

Hewitt, H., Fox-Kemper, B., Pearson, B., Roberts, M., and Klocke, D. (2022). The small scales of the ocean may hold the key to surprises. Nature Climate Change, 12, 496-499. doi: 10.1038/s41558-022-01386-6

Hobday, A. J., Alexander, L. V., Perkins, S. E., Smale, D. A., Straub, S. C., Oliver, E. C. J., Benthuysen, J. A., Burrows, M. T., Donat, M. G., Feng, M., Holbrook, N. J., Moore, P. J., Scannell, H. A., Sen Gupta, A., & Wernberg, T. (2016). A hierarchical approach to defining marine heatwaves. Progress in Oceanography, 141, 227- 238. https://doi.org/10.1016/j.pocean.2015.12.014

Hogg, A. McC., Meredith, M. P., Chambers, D. P., Abrahamsen, E. P., Hughes, C. W., & Morrison, A. K. (2015). Recent trends in the Southern Ocean eddy field. Journal of Geophysical Research: Oceans, 120(1), 257- 267. https://doi.org/10.1002/2014JC010470

Holbrook, N. J., Sen Gupta, A., Oliver, E. C. J., Hobday, A. J., Benthuysen, J. A., Scannell, H. A., Smale, D. A., & Wernberg, T. (2020). Keeping pace with marine heatwaves. Nature Reviews Earth & Environment, 1(9), 482- 493. https://doi.org/10.1038/s43017-020-0068-4

Huang, B., & Shukla, J. (2008). Interannual variability of the South Indian Ocean in observations and a coupled model. INDIAN J. MAR. SCI., 37(1), 23.

Huguenin, M.F., Holmes, R.M. & England, M.H. (2022). Drivers and distribution of global ocean heat uptake over the last half century. Nat Commun 13, 4921. https://doi.org/10.1038/s41467-022-32540-5

Hunt, B. P. V., Pakhomov, E. A., and McQuaid, C. D. (2001). Short-term variation and long-term changes in the oceanographic environment and zooplankton community in the vicinity of a sub-Antarctic archipelago. Marine Biology, 138, 369-381. https://doi.org/10.1007/s002270000467

IPCC (2022). Summary for Policymakers. In: Climate Change 2022: Mitigation of Climate Change. Contribution of Working Group III to the Sixth Assessment Report of the Intergovernmental Panel on

Climate Change [P.R. Shukla, J. Skea, R. Slade, A. Al Khourdajie, R. van Diemen, D. McCollum, M. Pathak, S. Some, P. Vyas, R. Fradera, M. Belkacemi, A. Hasija, G. Lisboa, S. Luz, J. Malley, (eds.)]. Cambridge University Press, Cambridge, UK and New York, NY, USA. doi: 10.1017/9781009157926.001

Jones, K. R., Watson, J. E. M., Possingham, H. P., & Klein, C. J. (2016). Incorporating climate change into spatial conservation prioritisation : A review. Biological Conservation, 194, 121 - 130. https://doi.org/10.1016/j.biocon.2015.12.008

Kock, K.-H., & Everson, I. (2003). Shedding new light on the life cycle of mackerel icefish in the Southern Ocean. Journal of Fish Biology, 63(1), 1 - 21. https://doi.org/10.1046/j.1095-8649.2003.00150.x

Kostianoy, A. G., Ginzburg, A. I., Frankignoulle, M., & Delille, B. (2004). Fronts in the Southern Indian Ocean as inferred from satellite sea surface temperature data. Journal of Marine Systems, 45(1), 55 - 73. https://doi.org/10.1016/j.jmarsys.2003.09.004

Kravtsov, S., Grimm, C., & Gu, S. (2018). Global-scale multidecadal variability missing in state-of-the-art climate models. Npj Climate and Atmospheric Science, 1(1), 1 - 10. https://doi.org/10.1038/s41612-018-0044-6

Kuhlbrodt, T., Jones, C. G., Sellar, A., Storkey, D., Blockley, E., Stringer, M., Hill, R., Graham, T., Ridley, J., Blaker, A., Calvert, D., Copsey, D., Ellis, R., Hewitt, H., Hyder, P., Ineson, S., Mulcahy, J., Siahaan, A., & Walton, J. (2018). The Low-Resolution Version of HadGEM3 GC3.1 : Development and Evaluation for Global Climate. Journal of Advances in Modeling Earth Systems, 10(11), 2865 - 2888. https://doi.org/10.1029/2018MS001370

Kwiatkowski, L., Torres, O., Bopp, L., Aumont, O., Chamberlain, M., Christian, J. R., Dunne, J. P., Gehlen, M., Ilyina, T., John, J. G., Lenton, A., Li, H., Lovenduski, N. S., Orr, J. C., Palmieri, J., Santana-Falcón, Y., Schwinger, J., Séférian, R., Stock, C. A., … Ziehn, T. (2020). Twenty-first century ocean warming, acidification, deoxygenation, and upper-ocean nutrient and primary production decline from

CMIP6 model projections. Biogeosciences, 17(13), 3439- 3470. https://doi.org/10.5194/bg-17-3439-2020

Le Bars, D., Viebahn, J. P., & Dijkstra, H. A. (2016). A Southern Ocean mode of multidecadal variability. Geophysical Research Letters, 43(5), 2102- 2110. https://doi.org/10.1002/2016GL068177

Lee, J.-Y., J. Marotzke, G. Bala, L. Cao, S. Corti, J.P. Dunne, F. Engelbrecht, E. Fischer, J.C. Fyfe, C. Jones, A. Maycock, J. Mutemi, O. Ndiaye, S. Panickal, and T. Zhou (2021). Future Global Climate: Scenario-Based Projections and NearTerm Information. In Climate Change 2021: The Physical Science Basis. Contribution of Working Group I to the Sixth Assessment Report of the Intergovernmental Panel on Climate Change [Masson-Delmotte, V., P. Zhai, A. Pirani, S.L. Connors, C. Péan, S. Berger, N. Caud, Y. Chen, L. Goldfarb, M.I. Gomis, M. Huang, K. Leitzell, E. Lonnoy, J.B.R. Matthews, T.K. Maycock, T. Waterfield, O. Yelekçi, R. Yu, and B. Zhou (eds.)]. Cambridge University Press, Cambridge, United Kingdom and New York, NY, USA, pp. 553–672, doi:10.1017/9781009157896.006.

Lin, X., Zhai, X., Wang, Z., & Munday, D. R. (2018). Mean, Variability, and Trend of Southern Ocean Wind Stress : Role of Wind Fluctuations. Journal of Climate, 31(9), 3557- 3573. https://doi.org/10.1175/JCLI-D-17-0481.1

Llovel, W., & Terray, L. (2016). Observed southern upper-ocean warming over 2005–2014 and associated mechanisms. Environmental Research Letters, 11(12), 124023. https://doi.org/10.1088/1748-9326/11/12/124023

Loarie, S. R., Duffy, P. B., Hamilton, H., Asner, G. P., Field, C. B., & Ackerly, D. D. (2009). The velocity of climate change. Nature, 462(7276), 1052- 1055. https://doi.org/10.1038/nature08649

Lovato, T., Peano, D., Butenschön, M., Materia, S., Iovino, D., Scoccimarro, E., Fogli, P. G., Cherchi, A., Bellucci, A., Gualdi, S., Masina, S., & Navarra, A. (2022). CMIP6 Simulations With the CMCC Earth System Model (CMCC-ESM2). Journal of Advances in Modeling Earth Systems, 14(3), e2021MS002814. https://doi.org/10.1029/2021MS002814

Lutjeharms, J. R. E. (Éd.). (2006). The Agulhas return flow. In The Agulhas Current (p. 209‑231). Springer. https://doi.org/10.1007/3-540-37212-1_7

Ma, J., Feng, M., Lan, J. and Hu, D., 2020. Projected future changes of meridional heat transport and heat balance of the Indian Ocean. Geophysical Research Letters, 47(4), p.e2019GL086803

Makhado, A.B., Lowther, A., Koubbi, P., Ansorge, I., Brooks,C., Cotté, C., Crawford, R., Dlulisa, S., d'Ovidio, F., Fawcet, S., Freeman, D., Grant, S., Huggett, J., Hindell, M., Hulley,P.A., Kirkman, S., Lamont, T., Lombard, M., Masothla, M.J., Lea, M.-A., Oosthuizen,W.C., Orgeret, F., Reisinger, R., Samaai, T., Sergi, S., Swadling, K., Somhlaba, S., Van de Putte, A., Von de Meden, C., and Yemane, D. (2019). Expert Workshop on Pelagic Spatial Planning for the eastern subantarctic region (Domains 4, 5 and 6). SC-CAMLR-38/BG/29.

Martínez-Moreno, J., Hogg, A. McC., Kiss, A. E., Constantinou, N. C., & Morrison, A. K. (2019). Kinetic Energy of Eddy-Like Features From Sea Surface Altimetry. Journal of Advances in Modeling Earth Systems, 11(10), 3090‑3105. https://doi.org/10.1029/2019MS001769

Martínez-Moreno, J., Hogg, A. M., England, M. H., Constantinou, N. C., Kiss, A. E., & Morrison, A. K. (2021). Global changes in oceanic mesoscale currents over the satellite altimetry record. Nature Climate Change, 11(5), 397‑403. https://doi.org/10.1038/s41558-021-01006-9

Matsuno, K., Wallis, J. R., Kawaguchi, S., Bestley, S. and Swadling, K. M. (2020). Zooplankton community structure and dominant copepod population structure on the southern Kerguelen Plateau during summer 2016. Deep-Sea Research II, 174, 104788. https://doi.org/10.1016/j.dsr2.2020.104788

Mauritsen, T., Bader, J., Becker, T., Behrens, J., Bittner, M., Brokopf, R., Brovkin, V., Claussen, M., Crueger, T., Esch, M., Fast, I., Fiedler, S., Fläschner, D., Gayler, V., Giorgetta, M., Goll, D. S., Haak, H., Hagemann, S., Hedemann, C., … Roeckner, E. (2019). Developments in the MPI-M Earth System Model version 1.2 (MPI-ESM1.2) and Its Response to Increasing CO2. Journal of Advances in Modeling Earth Systems, 11(4), 998‑1038. https://doi.org/10.1029/2018MS001400

Maxwell, S. M., Gjerde, K. M., Conners, M. G., & Crowder, L. B. (2020). Mobile protected areas for biodiversity on the high seas. Science, 367(6475), 252‐254. https://doi.org/10.1126/science.aaz9327

Meredith, M., M. Sommerkorn, S. Cassotta, C. Derksen, A. Ekaykin, A. Hollowed, G. Kofinas, A. Mackintosh, J. Melbourne-Thomas, M.M.C. Muelbert, G. Ottersen, H. Pritchard, and E.A.G. Schuur (2019). Polar Regions. In: IPCC Special Report on the Ocean and Cryosphere in a Changing Climate [H.-O. Pörtner, D.C. Roberts, V. Masson-Delmotte, P. Zhai, M. Tignor, E. Poloczanska, K. Mintenbeck, A. Alegría, M. Nicolai, A. Okem, J. Petzold, B. Rama, N.M. Weyer (eds.)]. Cambridge University Press, Cambridge, UK and New York, NY, USA, pp. 203–320. https://doi.org/10.1017/9781009157964.005.

Mills, K. E., Pershing, A. J., Brown C. J., Chen, Y., Chiang, F.-S., Holland, D. S., Lehuta, S., Nye, J. A., Sun, J. C., Thomas, A. C., & Wahle, R. A. (2013). Fisheries Management in a Changing Climate : Lessons from the 2012 Ocean Heat Wave in the Northwest Atlantic. Oceanography, 26(2), 191‐195.

Mishra, R. K., Naik, R. K., Venkataramana, V., Jena, B., AnilKumar, N., Soares, M. A., Sarkar, A. and Singh, A. (2020). Phytoplankton biomass and community composition in the front zones of Southern Ocean. Deep-Sea Research II, 178, 104799. https://doi.org/10.1016/j.dsr2.2020.104799

Morrison, A. K., Griffies, S. M., Winton, M., Anderson, W. G., & Sarmiento, J. L. (2016). Mechanisms of Southern Ocean Heat Uptake and Transport in a Global Eddying Climate Model. Journal of Climate, 29(6), 2059‐2075. https://doi.org/10.1175/JCLI-D-15-0579.1

Müller, W. A., Jungclaus, J. H., Mauritsen, T., Baehr, J., Bittner, M., Budich, R., Bunzel, F., Esch, M., Ghosh, R., Haak, H., Ilyina, T., Kleine, T., Kornblueh, L., Li, H., Modali, K., Notz, D., Pohlmann, H., Roeckner, E., Stemmler, I., … Marotzke, J. (2018). A Higher-resolution Version of the Max Planck Institute Earth System Model (MPI-ESM1.2-HR). Journal of Advances in Modeling Earth Systems, 10(7), 1383‐1413. https://doi.org/10.1029/2017MS001217

Oliver, E. C. J. (2019a). Mean warming not variability drives marine heatwave trends. Climate Dynamics, 53(3), 1653‐1659. https://doi.org/10.1007/s00382-019-04707-2

Oliver, E. C. J., Burrows, M. T., Donat, M. G., Sen Gupta, A., Alexander, L. V., Perkins-Kirkpatrick, S. E., Benthuysen, J. A., Hobday, A. J., Holbrook, N. J., Moore, P. J., Thomsen, M. S., Wernberg, T., & Smale, D. A. (2019b). Projected Marine Heatwaves in the 21st Century and the Potential for Ecological Impact. Frontiers in Marine Science, 6, 734. https://doi.org/10.3389/fmars.2019.00734

O'Neill, B. C., Tebaldi, C., van Vuuren, D. P., Eyring, V., Friedlingstein, P., Hurtt, G., Knutti, R., Kriegler, E., Lamarque, J.-F., Lowe, J., Meehl, G. A., Moss, R., Riahi, K., & Sanderson, B. M. (2016). The Scenario Model Intercomparison Project (ScenarioMIP) for CMIP6. Geoscientific Model Development, 9(9), 3461‐3482. https://doi.org/10.5194/gmd-9-3461-2016

O'Neill, B. C., Kriegler, E., Ebi, K. L., Kemp-Benedict, E., Riahi, K., Rothman, D. S., van Ruijven, B. J., van Vuuren, D. P., Birkmann, J., Kok, K., Levy, M., & Solecki, W. (2017). The roads ahead: Narratives for shared socioeconomic pathways describing world futures in the 21st century. Global Environmental Change, 42, 169‐180. https://doi.org/10.1016/j.gloenvcha.2015.01.004

Ortuño Crespo, G., Mossop, J., Dunn, D., Gjerde, K., Hazen, E., Reygondeau, G., Warner, R., Tittensor, D., & Halpin, P. (2020). Beyond static spatial management: Scientific and legal considerations for dynamic management in the high seas. Marine Policy, 122, 104102. https://doi.org/10.1016/j.marpol.2020.104102

Park Y.-H., Gambéroni, L., and Charriaud, E. (1991). Frontal structure and transport of the Antarctic Circumpolar Current in the south Indian Ocean sector, 40-80°E. Marine Chemistry, 35, 45-62. https://doi.org/10.1016/S0304-4203(09)90007-X

Park, Y.-H., Gamberoni, L., and Charriaud, E. (1993). Frontal structure, water masses, and circulation in the Crozet Basin. J. Geophys. Res., 98(C7), 12361– 12385. doi:10.1029/93JC00938

Park, Y.-H., Roquet, F., Durand, I. and Fuda, J.-L. (2008). Large-scale circulation over and around the Northern Kerguelen Plateau. Deep Sea Research II, 55(5-7), 566-581. https://doi.org/10.1016/j.dsr2.2007.12.030

Park, Y.-H., Vivier, F., Roquet, F., and Kestenare, E. (2009). Direct observations of the ACC transport across the Kerguelen Plateau. Geophys. Res. Lett., 36, L18603. doi:10.1029/2009GL039617.

Park Y.-H., and Durand, I. (2019). Altimetry-derived Antarctic Circumpolar Current Fronts. SEANOE. https://doi.org/10.17882/59800

Park Y.- H., Park T., Kim T.- W., Lee S.- H., Hong C.- S., Lee J.- H., Rio M.- H., Pujol M.- I., Ballarotta M., Durand I., Provost C. (2019). Observations of the Antarctic Circumpolar Current over the Udintsev Fracture Zone, the narrowest choke point in the Southern Ocean. Journal of Geophysical Research: Oceans, 124, 4511-4528. https://doi.org/10.1029/2019JC015024

Patara, L., Böning, C. W., & Biastoch, A. (2016). Variability and trends in Southern Ocean eddy activity in 1/12° ocean model simulations. Geophysical Research Letters, 43(9), 4517‐4523. https://doi.org/10.1002/2016GL069026

Pietri, A., Colas, F., Mogollon, R., Tam, J., & Gutierrez, D. (2021). Marine heatwaves in the Humboldt current system : From 5-day localized warming to year-long El Niños. Scientific Reports, 11(1), 1‐12. https://doi.org/10.1038/s41598-021-00340-4

Pilo, G. S., Holbrook, N. J., Kiss, A. E., & Hogg, A. M. (2019). Sensitivity of Marine Heatwave Metrics to Ocean Model Resolution. Geophysical Research Letters, 46(24), 14604‐14612. https://doi.org/10.1029/2019GL084928

Plecha, S. M., & Soares, P. M. M. (2020). Global marine heatwave events using the new CMIP6 multi-model ensemble : From shortcomings in present climate to future projections. Environmental Research Letters, 15(12). https://doi.org/10.1088/1748-9326/abc847

Pütz, K. (2002). Spatial and Temporal Variability in the Foraging Areas of Breeding King Penguins. The Condor, 104(3), 528‐538. https://doi.org/10.1093/condor/104.3.528

Qiu, Z., Qiao, F., Jang, C. J., Zhang, L., & Song, Z. (2021). Evaluation and projection of global marine heatwaves based on CMIP6 models. Deep Sea Research Part II: Topical Studies in Oceanography, 194, 104998. https://doi.org/10.1016/j.dsr2.2021.104998

Raäisaänen, J. (2007). How reliable are climate models? Tellus A: Dynamic Meteorology and Oceanography, 59(1), 2‐29. https://doi.org/10.1111/j.1600-0870.2006.00211.x

Reisinger, R. R., Corney, S., Raymond, B., Lombard, A. T., Bester, M. N., Crawford, R. J. M., Davies, D., de Bruyn, P. J. N., Dilley, B. J., Kirkman, S. P., Makhado, A. B., Ryan, P. G., Schoombie, S., Stevens, K. L., Tosh, C. A., Wege, M., Whitehead, T. O., Sumner, M. D., Wotherspoon, S., … Pistorius, P. A. (2022). Habitat model forecasts suggest potential redistribution of marine predators in the southern Indian Ocean. Diversity and Distributions, 28(1), 142‐159. https://doi.org/10.1111/ddi.13447

Reygondeau, G., Cheung, W. W. L., Wabnitz, C. C. C., Lam, V. W. Y., Frölicher, T., & Maury, O. (2020). Climate Change-Induced Emergence of Novel Biogeochemical Provinces. Frontiers in Marine Science, 7, 657. https://doi.org/10.3389/fmars.2020.00657

Reynolds, Richard W., Thomas M. Smith, Chunying Liu, Dudley B. Chelton, Kenneth S. Casey, Michael G. Schlax (2007). Daily High-Resolution-Blended Analyses for Sea Surface Temperature. J. Climate, 20, 5473-5496. Reynolds, Richard W., Thomas M. Smith, Chunying Liu, Dudley B. Chelton, Kenneth S. Casey, Michael G. Schlax, 2007: Daily High-Resolution-Blended Analyses for Sea Surface Temperature. J. Climate, 20, 5473-5496.

Riahi, K., van Vuuren, D. P., Kriegler, E., Edmonds, J., O'Neill, B. C., Fujimori, S., Bauer, N., Calvin, K., Dellink, R., Fricko, O., Lutz, W., Popp, A., Cuaresma, J. C., Kc, S., Leimbach, M., Jiang, L., Kram, T., Rao, S., Emmerling, J., … Tavoni, M. (2017). The Shared Socioeconomic Pathways and their energy, land use, and greenhouse gas emissions implications : An overview. Global Environmental Change, 42, 153‐168. https://doi.org/10.1016/j.gloenvcha.2016.05.009

Rintoul, S. R. and Naveira Garabato, A.C. (2013). Chapter 18 - Dynamics of the Southern Ocean circulation. In G. Siedler, S. M. Griffies, J. Gould, & J. A. Church (Eds.), International geophysics,

ocean circulation and climate (Vol. 103, pp. 471– 492). Waltham, MA: Academic Press. https://doi.org/10.1016/B978-0-12-391851-2.00018-0

Roemmich, D., Church, J., Gilson, J., Monselesan, D., Sutton, P., & Wijffels, S. (2015). Unabated planetary warming and its ocean structure since 2006. Nature Climate Change, 5(3), 240‐245. https://doi.org/10.1038/nclimate2513

Rong, X.-Y., Li, J., Chen, H.-M., Xin, Y.-F., Su, J.-Z., Hua, L.-J., & Zhang, Z.-Q. (2019). Introduction of CAMS-CSM model and its participation in CMIP6. Advances in Climate Change Research, 15(5), 540. https://doi.org/10.12006/j.issn.1673-1719.2019.186

Roquet, F., Park, Y-H., Guinet, C., Bailleul, F., and Charassin, J-B. (2009). Observations of the Fawn Trough Current over the Kerguelen Plateau from instrumented elephant seals. Journal of Marine Systems, 78, 377-393. doi:10.1016/j.jmarsys.2008.11.017

Saenko, O. A., Yang, D., & Gregory, J. M. (2018). Impact of Mesoscale Eddy Transfer on Heat Uptake in an Eddy-Parameterizing Ocean Model. Journal of Climate, 31(20), 8589‐8606. https://doi.org/10.1175/JCLI-D-18-0186.1

Sallée, J. B., Speer, K. G., & Rintoul, S. R. (2010). Zonally asymmetric response of the Southern Ocean mixed-layer depth to the Southern Annular Mode. Nature Geoscience, 3(4), 273‐279. https://doi.org/10.1038/ngeo812

Sallée, J.-B. (2018). Southern Ocean Warming. Oceanography, 31(2), 52‐62. JSTOR.

Scannell, H. A., Pershing, A. J., Alexander, M. A., Thomas, A. C., & Mills, K. E. (2016). Frequency of marine heatwaves in the North Atlantic and North Pacific since 1950. Geophysical Research Letters, 43(5), 2069‐2076. https://doi.org/10.1002/2015GL067308

Schlegel, R. W., Oliver, E. C. J., Hobday, A. J., & Smit, A. J. (2019). Detecting Marine Heatwaves With Sub-Optimal Data. Frontiers in Marine Science, 6, 737. https://doi.org/10.3389/fmars.2019.00737

Schmidt, C., Schwarzkopf, F. U., Rühs, S., & Biastoch, A. (2021). Characteristics and robustness of Agulhas leakage estimates : An inter-comparison study of Lagrangian methods. Ocean Science, 17(4), 1067‐ 1080. https://doi.org/10.5194/os-17-1067-2021

Séférian, R., Nabat, P., Michou, M., Saint-Martin, D., Voldoire, A., Colin, J., Decharme, B., Delire, C., Berthet, S., Chevallier, M., Sénési, S., Franchistéguy, L., Vial, J., Mallet, M., Joetzjer, E., Ge offroy, O., Guérémy, J.-F., Moine, M.-P., M'Sadek, R., Ribes, A., Rocher, M., Roehrig, R., Salas-y-Mélia, D., Sanchez, E., Terray, L., Valcke, S., Waldman, R., Aumont, O., Bopp, L., Deshayes, J., Éthé, C., and Madec, G. (2019). Evaluation of CNRM Earth Sys tem model, CNRM-ESM2-1: role of Earth system processes in present-day and future climate. J. Adv. Model. Earth Syst., 11, 4182–4227. https://doi.org/10.1029/2019MS001791

Sellar, A. A., Jones, C. G., Mulcahy, J., Tang, Y., Yool, A., Wilt shire, A., O'connor, F. M., Stringer, M., Hill, R., Palmieri, J., Woodward, S., Mora, L., Kuhlbrodt, T., Rumbold, S., Kelley, D. I., Ellis, R., Johnson, C. E., Walton, J., Abraham, N. L., Andrews, M. B., Andrews, T., Archibald, A. T., Berthou, S., Burke, E., Blockley, E., Carslaw, K., Dalvi, M., Edwards, J., Folberth, G. A., Gedney, N., Griffiths, P. T., Harper, A. B., Hendry, M. A., He witt, A. J., Johnson, B., Jones, A., Jones, C. D., Keeble, J., Liddi coat, S., Morgenstern, O., Parker, R. J., Predoi, V., Robertson, E., Siahaan, A., Smith, R. S., Swaminathan, R., Woodhouse, M. T., Zeng, G., and Zerroukat, M.: UKESM1: Description and evaluation of the UK Earth System Model (2019). J. Adv. Model. Earth Syst., 11, 4513–4558, https://doi.org/10.1029/2019MS001739

Sen Gupta, A., Brown, J. N., Jourdain, N. C., van Sebille, E., Ganachaud, A., & Vergés, A. (2015). Episodic and non-uniform shifts of thermal habitats in a warming ocean. Deep Sea Research Part II: Topical Studies in Oceanography, 113, 59‐ 72. https://doi.org/10.1016/j.dsr2.2013.12.002

Sen Gupta, A., Stellema, A., Pontes, G. M., Taschetto, A. S., Vergés, A., & Rossi, V. (2021). Future changes to the upper ocean Western Boundary Currents across two generations of climate models. Scientific Reports, 11(1), 9538. https://doi.org/10.1038/s41598-021-88934-w

Siegelman, L., Klein, P., Rivière, P., Thompson, A. F., Torres, H. S., Flexas, M., & Menemenlis, D. (2020). Enhanced upward heat transport at deep submesoscale ocean fronts. Nature Geoscience, 13(1), 50–55. https://doi.org/10.1038/s41561-019-0489-1

Smale, D. A., & Wernberg, T. (2013). Extreme climatic event drives range contraction of a habitat-forming species. Proceedings of the Royal Society B: Biological Sciences, 280(1754), 20122829. https://doi.org/10.1098/rspb.2012.2829

Smale DA, Wernberg T, & Vanderklift MA. (2017). Regional-scale variability in the response of benthic macroinvertebrate assemblages to a marine heatwave. Marine Ecology Progress Series, 568, 17–30.

Stellema, A., Sen Gupta, A., & Taschetto, A. S. (2019). Projected slow down of South Indian Ocean circulation. Scientific Reports, 9(1), 17705. https://doi.org/10.1038/s41598-019-54092-3

Su, Z., Pilo, G. S., Corney, S., Holbrook, N. J., Mori, M., & Ziegler, P. (2021). Characterizing Marine Heatwaves in the Kerguelen Plateau Region. Frontiers in Marine Science, 7, 1119. https://doi.org/10.3389/fmars.2020.531297

Swart, N. C., Cole, J. N. S., Kharin, V. V., Lazare, M., Scinocca, J. F., Gillett, N. P., Anstey, J., Arora, V., Christian, J. R., Hanna, S., Jiao, Y., Lee, W. G., Majaess, F., Saenko, O. A., Seiler, C., Seinen, C., Shao, A., Sigmond, M., Solheim, L., … Winter, B. (2019). The Canadian Earth System Model version 5 (CanESM5.0.3). Geoscientific Model Development, 12(11), 4823–4873. https://doi.org/10.5194/gmd-12-4823-2019

Tatebe, H., Ogura, T., Nitta, T., Komuro, Y., Ogochi, K., Takemura, T., Sudo, K., Sekiguchi, M., Abe, M., Saito, F., Chikira, M., Watanabe, S., Mori, M., Hirota, N., Kawatani, Y., Mochizuki, T., Yoshimura, K., Takata, K., O'ishi, R., … Kimoto, M. (2019). Description and basic evaluation of simulated mean state, internal variability, and climate sensitivity in MIROC6. Geoscientific Model Development, 12(7), 2727–2765. https://doi.org/10.5194/gmd-12-2727-2019

Tittensor, D. P., Beger, M., Boerder, K., Boyce, D. G., Cavanagh, R. D., Cosandey-Godin, A., Crespo, G. O., Dunn, D. C., Ghiffary, W., Grant, S. M., Hannah, L., Halpin, P. N., Harfoot, M., Heaslip, S. G., Jeffery, N. W., Kingston, N., Lotze, H. K., McGowan, J., McLeod, E., … Worm, B. (2019). Integrating climate adaptation and biodiversity conservation in the global ocean. Science Advances. https://doi.org/10.1126/sciadv.aay9969

van Wijk, E. M., Rintoul, S. R., Ronai, B. M. and Williams, G. D. (2010). Regional circulation around Heard and McDonald Islands and through the Fawn Trough, central Kerguelen Plateau. Deep-Sea Research I, 57, 653-669. doi:10.1016/j.dsr.2010.03.001

VanDerWal, J., Murphy, H. T., Kutt, A. S., Perkins, G. C., Bateman, B. L., Perry, J. J., & Reside, A. E. (2013). Focus on poleward shifts in species' distribution underestimates the fingerprint of climate change. Nature Climate Change, 3(3), 239‐ 243. https://doi.org/10.1038/nclimate1688

Venkataramana, V., Anilkumar, N. Swadling, K., Mishra, R. K., Tripathy, S. C., Sarkar, A., Augusta, S. M., Sabu, P. and Pillai, H. (2020). Distribution of zooplankton in the Indian sector of the Southern Ocean. Antarctic Science, 32(3), 168-179. doi:10.1017/S0954102019000579

Vivier, F., Park, Y-H., Sekma, H., and Le Sommer, J. (2015). Variability of the Antarctic Circumpolar Current transport through the Fawn Trough, Kerguelen Plateau. Deep-Sea Research II, 114, 12-26. http://dx.doi.org/10.1016/j.dsr2.2014.01.017

Voldoire, A., Saint-Martin, D., Sénési, S., Decharme, B., Alias, A., Chevallier, M., Colin, J., Guérémy, J.-F., Michou, M., Moine, M.-P., Nabat, P., Roehrig, R., Salas y Mélia, D., Séférian, R., Valcke, S., Beau, I., Belamari, S., Berthet, S., Cassou, C., … Waldman, R. (2019). Evaluation of CMIP6 DECK Experiments With CNRM-CM6-1. Journal of Advances in Modeling Earth Systems, 11(7), 2177‐ 2213. https://doi.org/10.1029/2019MS001683

Wiens, J. A., & Bachelet, D. (2010). Matching the Multiple Scales of Conservation with the Multiple Scales of Climate Change. Conservation Biology, 24(1), 51‐ 62. https://doi.org/10.1111/j.1523-1739.2009.01409.x

Wilson, K. L., Tittensor, D. P., Worm, B., & Lotze, H. K. (2020). Incorporating climate change adaptation into marine protected area planning. Global Change Biology, 26(6), 3251‐3267. https://doi.org/10.1111/gcb.15094

Wu, T., Lu, Y., Fang, Y., Xin, X., Li, L., Li, W., Jie, W., Zhang, J., Liu, Y., Zhang, L., Zhang, F., Zhang, Y., Wu, F., Li, J., Chu, M., Wang, Z., Shi, X., Liu, X., Wei, M., … Liu, X. (2019). The Beijing Climate Center Climate System Model (BCC‐CSM): The main progress from CMIP5 to CMIP6. Geoscientific Model Development, 12(4), 1573‐1600. https://doi.org/10.5194/gmd-12-1573-2019

Yang, C., Leonelli, F. E., Marullo, S., Artale, V., Beggs, H., Nardelli, B. B., Chin, T. M., Toma, V. D., Good, S., Huang, B., Merchant, C. J., Sakurai, T., Santoleri, R., Vazquez‐Cuervo, J., Zhang, H.‐M., & Pisano, A. (2021). Sea Surface Temperature Intercomparison in the Framework of the Copernicus Climate Change Service (C3S). Journal of Climate, 34(13), 5257‐5283. https://doi.org/10.1175/JCLI-D-20-0793.1

Yukimoto, S., Kawai, H., Koshiro, T., Oshima, N., Yoshida, K., Urakawa, S., Tsujino, H., Deushi, M., Tanaka, T., Hosaka, M., Yabu, S., Yoshimura, H., Shindo, E., Mizuta, R., Obata, A., Adachi, Y., and Ishii, M. (2019). The Meteorological Research Institute Earth System Model version 2.0, MRI‐ESM2.0: Description and basic evaluation of the physical component, J. Meteorol. Soc. Jpn., 97, 931–965,, https://doi.org/10.2151/jmsj.2019‐051

Zhang, Y., Feng, M., Du, Y., Phillips, H. E., Bindoff, N. L., & McPhaden, M. J. (2018). Strengthened Indonesian throughflow drives decadal warming in the Southern Indian Ocean. Geophysical Research Letters, 45(12), 6167‐6175. https://doi.org/10.1029/2018GL078265

Ziehn, T., Chamberlain, M. A., Law, R. M., Lenton, A., Bodman, R. W., Dix, M., Stevens, L., Wang, Y.‐P., Srbinovsky, J., Ziehn, T., Chamberlain, M. A., Law, R. M., Lenton, A., Bodman, R. W., Dix, M., Stevens, L., Wang, Y.‐P., & Srbinovsky, J. (2020). The Australian Earth System Model: ACCESS‐ESM1.5. Journal of Southern Hemisphere Earth Systems Science, 70(1), 193‐214. https://doi.org/10.1071/ES19035

Appendix A: Supplementary Materials

Figure S1: List of models used for the timeshift approach analyses for both SSP 245 and SSP585.

For changes in temperature (yearly data) 22 models	**For MHW intensity (daily data) 17 models**
ACCESS-CM2	ACCESS-CM2
ACCESS-ESM1-5	ACCESS-ESM1-5
BCC-CMS2-MR	BCC-CMS2-MR
CAMS-CSM1-0	CanESM5
CanESM5	CESM2-WACCM
CanESM5-CanOE	CMCC-ESM2
CESM2-WACCM	CMCC-CM2-SR5
CMCC-ESM2	CNRM-CM6-1
CMCC-CM2-SR5	CNRM-CM6-1-HR
CNRM-CM6-1	GFDL-CM4
GFDL-CM4	EC-Earth3
GFDL-ESM4	IPSL-CM6A-LR
HadGEM3-GC31-LL	MIROC6
EC-Earth3-CC	MPI-ESM1-HR
EC-Earth3-Veg	MPI-ESM1-LR
IPSL-CM6A-LR	MRI-ESM2-0
MIROC-ES2L	NESM3
MPI-ESM1-HR	
MPI-ESM1-LR	
MRI-ESM2-0	
NESM3	
UKESM1-0-LL	

Figure S2 : Temperature trends between 1982 and 2019 in the Southern Indian Ocean (top panel), using linear regression on sea surface temperature, using OISST (left) and OSTIA (right) datasets. Timeseries of sea surface temperature for two areas (bottom panel): one west of the Southern Indian Ocean, covering Prince Edward Islands and Crozet (orange) and one north of Saint-Paul and Amsterdam (green) using OISST (full) and OSTIA (dashed) datasets

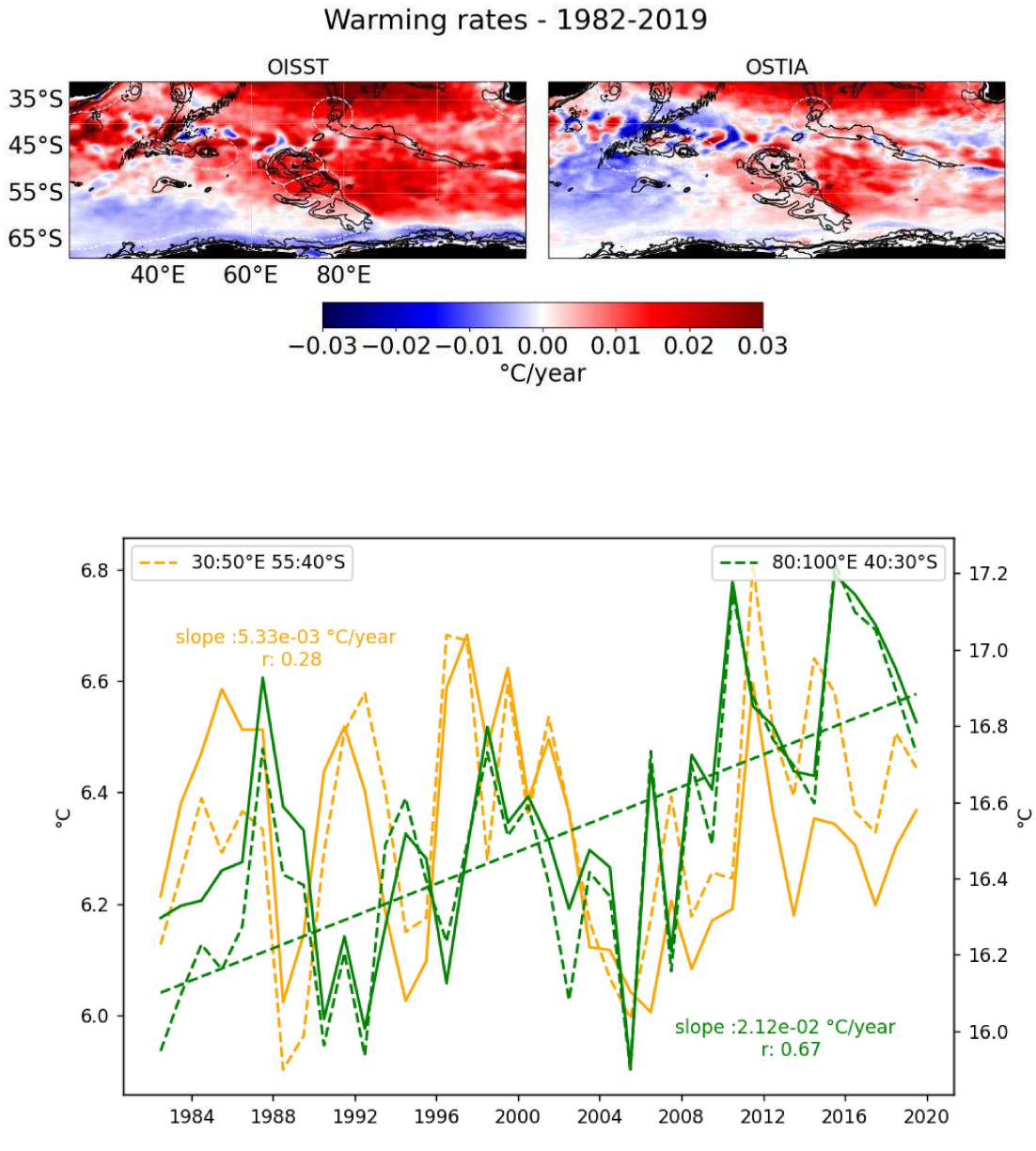

Figure S3: Warming rates between 1982-2019 for each of the 24 CMIP6 models studied.

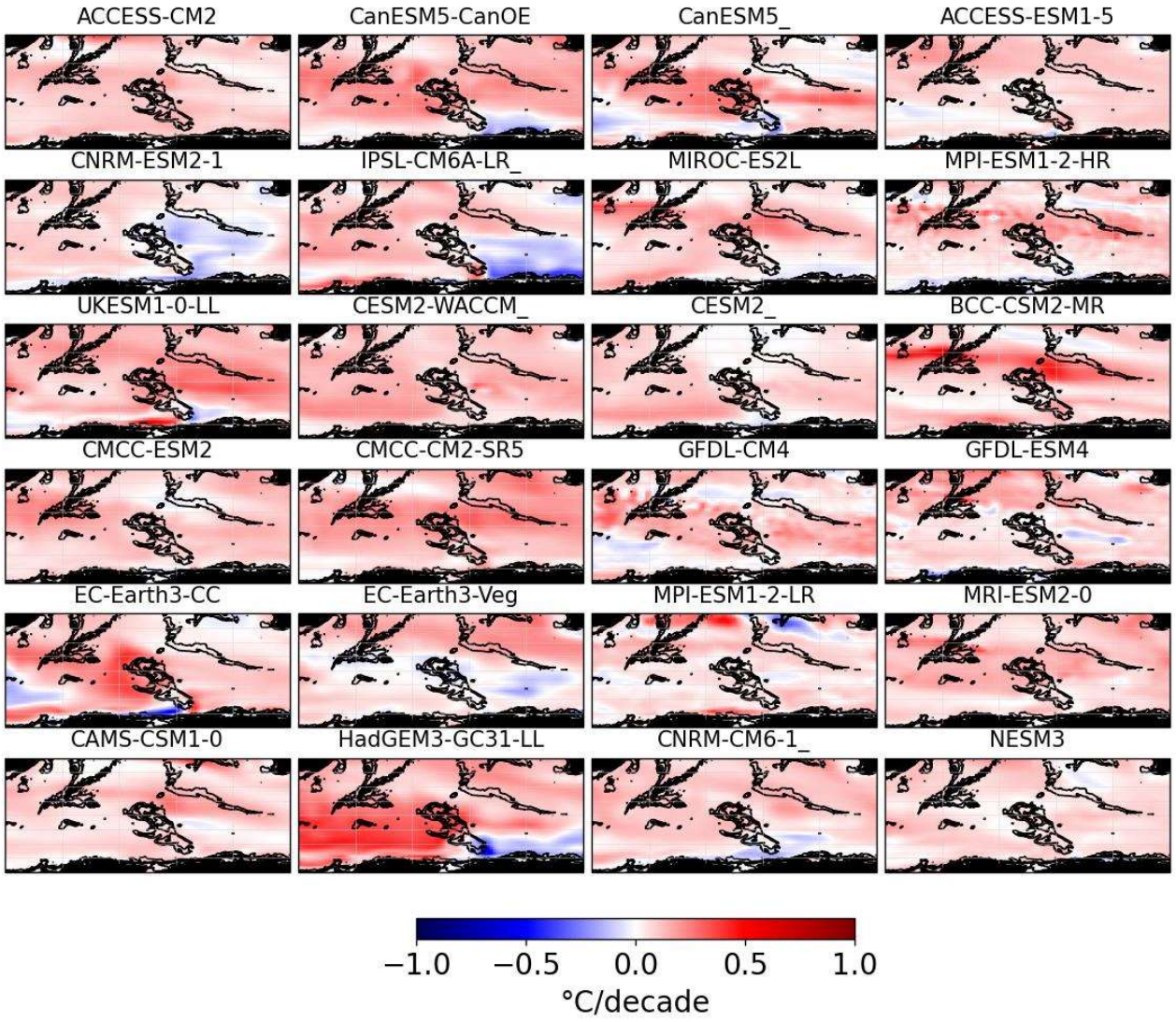

Figure S4: MHW intensity over 1984-2014 (90th percentile) for each of the 19 CMIP6 models studied.

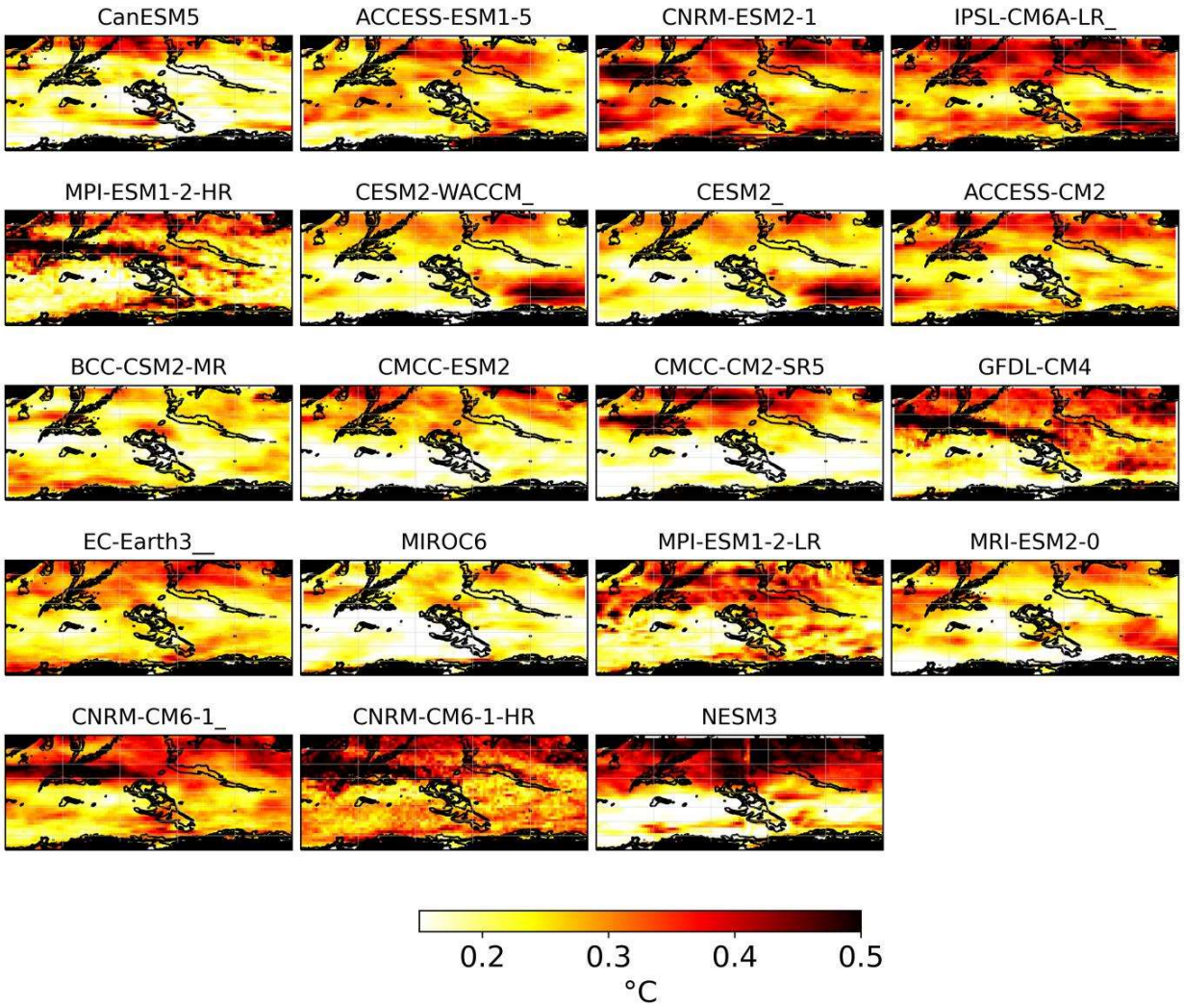

Figure S5 : (A) Warming trends between 1975 and 2015 of 10 IPSL-CM6A-LR members. (B) Change in surface temperature (2081-2100 minus 1995-2014) of the same 10 IPSL-CM6A-LR members under

SSP2-4.5. (C)Time series of mean Pearson correlation coefficient, as an indicator of spatial similarity,

for each 10 IPSL-CM6A-LR members relative to r1i1p1f1 member, under SSP2-4.5.

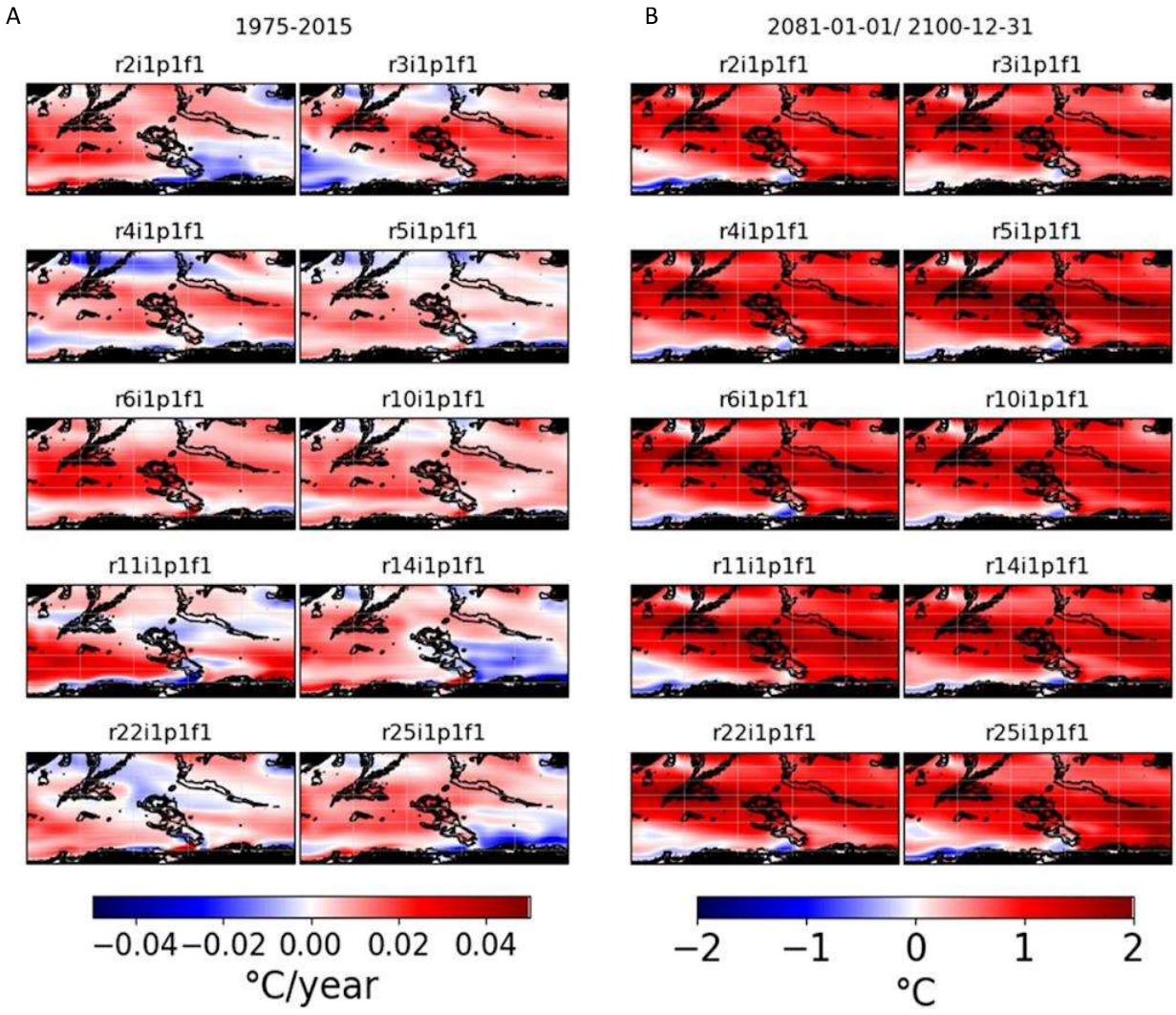

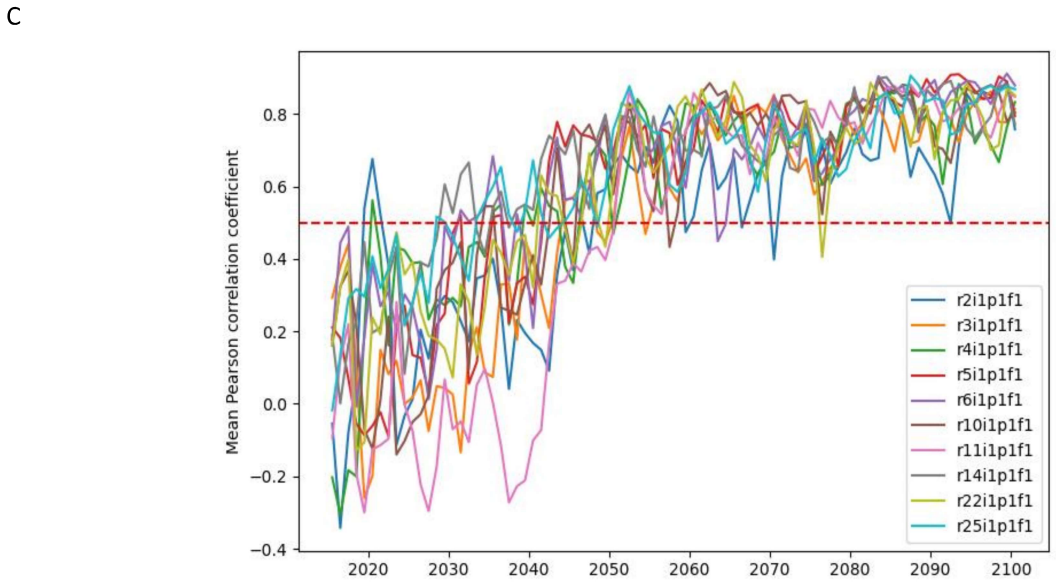

Figure S6: Relative increase in the mean (full) or spread (hatched) of the daily temperature distribution under SSP2-4.5 relative to historical period (1995-2014) from 19 CMIP6 models for 2021-2040 (near term, NT), 2041-2060 (mid term, MT) and 2081-2100 (long term, LT).

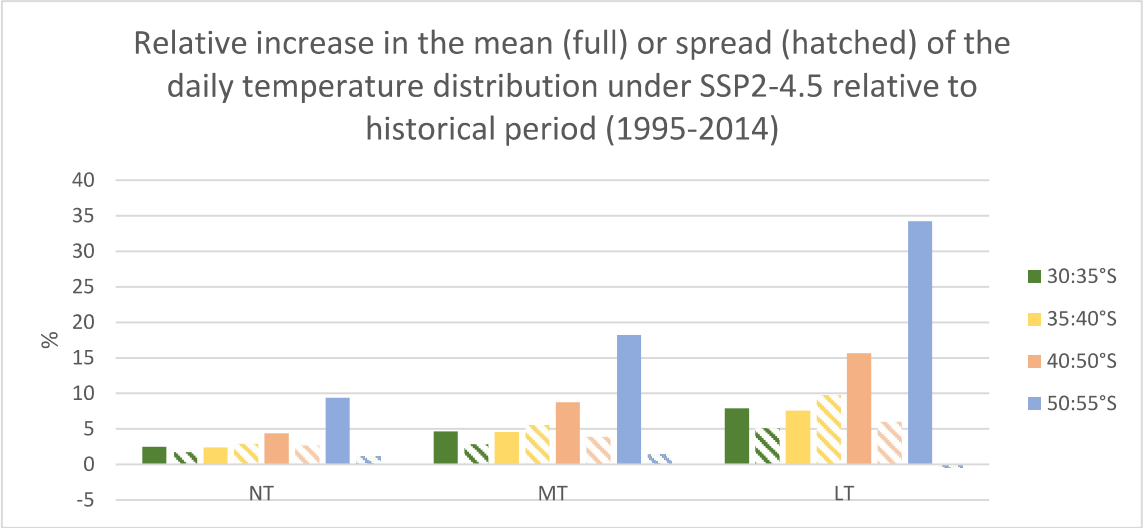

Figure S7: Relation between the change in surface temperature and MHW annual days for 20-year periods under SSP1-2.6 and SSP2-4.5 averaged over the area. Error bars correspond to intermodel variability.

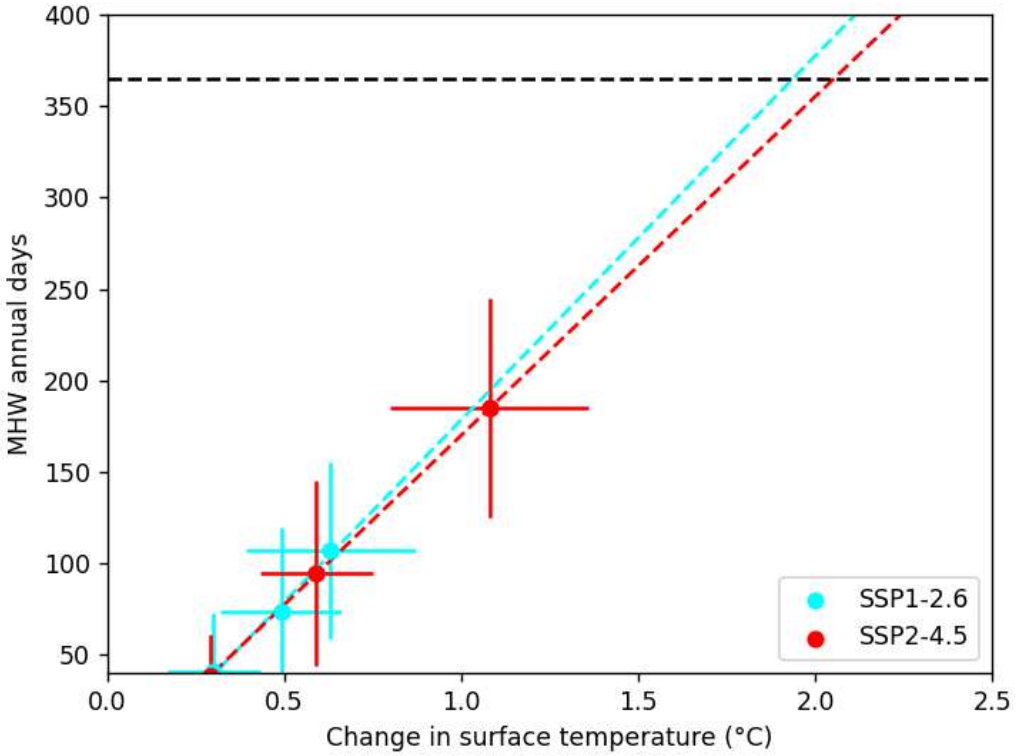

Figure S8: Change in surface temperature for the near-, mid- and long-terms under SSP2-4.5 for two high resolution models: MIP-ESM1-2-HR and GFDL-CM4.